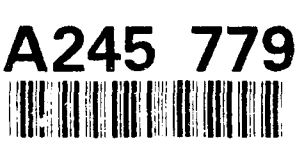

(2)

NAVAL POSTGRADUATE SCHOOL

Monterey, California

THESIS

THE EFFECT OF LATENT HEAT RELEASE
ON THE
ERICA IOP-5 CYCLONE

by

Frank W. Baker

September, 1991

Thesis Advisor: Patricia M. Pauley

Approved for public release; distribution is unlimited

REPORT DOCUMENTATION PAGE

1a. REPORT SECURITY CLASSIFICATION Unclassified	1b. RESTRICTIVE MARKINGS
2a. SECURITY CLASSIFICATION AUTHORITY	3. DISTRIBUTION/AVAILABILITY OF REPORT Approved for public release; distribution is unlimited.
2b. DECLASSIFICATION/DOWNGRADING SCHEDULE	
4. PERFORMING ORGANIZATION REPORT NUMBER(S)	5. MONITORING ORGANIZATION REPORT NUMBER(S)
6a. NAME OF PERFORMING ORGANIZATION Naval Postgraduate School 6b. OFFICE SYMBOL (*If applicable*) 35	7a. NAME OF MONITORING ORGANIZATION Naval Postgraduate School
6c. ADDRESS (*City, State, and ZIP Code*) Monterey, CA 93943-5000	7b. ADDRESS (*City, State, and ZIP Code*) Monterey, CA 93943-5000
8a. NAME OF FUNDING/SPONSORING ORGANIZATION 8b. OFFICE SYMBOL (*If applicable*)	9. PROCUREMENT INSTRUMENT IDENTIFICATION NUMBER
8c. ADDRESS (*City, State, and ZIP Code*)	10. SOURCE OF FUNDING NUMBERS Program Element No / Project No. / Task No / Work Unit Accession Number

11. TITLE (*Include Security Classification*)
THE EFFECT OF LATENT HEAT RELEASE ON THE ERICA IOP-5 CYCLONE

12. PERSONAL AUTHOR(S) Baker, Frank W.

13a. TYPE OF REPORT	13b. TIME COVERED	14. DATE OF REPORT (*year, month, day*)	15. PAGE COUNT
Master's Thesis	From To	1991 September	87

16. SUPPLEMENTARY NOTATION
The views expressed in this thesis are those of the author and do not reflect the official policy or position of the Department of Defense or the U.S. Government.

17. COSATI CODES			18. SUBJECT TERMS (*continue on reverse if necessary and identify by block number*)
FIELD	GROUP	SUBGROUP	latent heat release, rapid intensification, height tendency, ERICA

19. ABSTRACT (*continue on reverse if necessary and identify by block number*)

The effect of latent heat release on the development of a rapidly deepening extratropical cyclone that occurred during Intensive Observation Period (IOP) 5 (18-20 January 1989) of the Experiment on Rapidly Deepening Cyclones over the Atlantic (ERICA) is examined using a diagnostic height tendency equation. Data consist of Nested Grid Model (NGM) forecasts executed with and without latent heating feedback. Withholding latent heat release significantly decreased the intensity of not only the surface cyclone, but its associated 500 mb trough/ridge system as well. Propagation speed differed only slightly between the two forecasts, allowing the differences in intensification to be explored through height tendency differences between the two forecasts. Model results show that at 500 mb, latent heat release affects the height tendencies primarily through indirect means, chiefly by enhancing vorticity advection. Differential thermal advection and vertical advection of static stability tended to offset each other, as did vertical advection of vorticity and tilting effects. A height anomaly due to latent heat release was located downstream of the 500 mb trough and served as a focus for forcing differences associated with latent heating.

20. DISTRIBUTION/AVAILABILITY OF ABSTRACT	21. ABSTRACT SECURITY CLASSIFICATION	
☒ UNCLASSIFIED/UNLIMITED ☐ SAME AS REPORT ☐ DTIC USERS	Unclassified	
22a. NAME OF RESPONSIBLE INDIVIDUAL Patricia M. Pauley	22b. TELEPHONE (*Include Area code*) (408) 646-3275	22c. OFFICE SYMBOL 63PA

DD FORM 1473, 84 MAR 83 APR edition may be used until exhausted
All other editions are obsolete

Approved for public release; distribution is unlimited.

The Effect of Latent Heat Release
on the ERICA IOP-5 Cyclone

by

Frank W. Baker
Lieutenant, United States Navy
B.A., Pennsylvania State University, 1983

Submitted in partial fulfillment
of the requirements for the degree of

MASTER OF SCIENCE IN METEOROLOGY AND PHYSICAL OCEANOGRAPHY

from the

NAVAL POSTGRADUATE SCHOOL
September 1991

Author: _____
Frank W. Baker

Approved by: _____
Patricia M. Pauley, Thesis Advisor

_____
Carlyle H. Wash, Second Reader

_____
Robert L. Haney, Chairman
Department of Meteorology

ABSTRACT

The effect of latent heat release on the development of a rapidly deepening extratropical cyclone that occurred during Intensive Observation Period (IOP) 5 (18-20 January 1989) of the Experiment on Rapidly Deepening Cyclones over the Atlantic (ERICA) is examined using a diagnostic height tendency equation. Data consist of Nested Grid Model (NGM) forecasts executed with and without latent heating feedback. Withholding latent heat release significantly decreased the intensity of not only the surface cyclone, but its associated 500 mb trough/ridge system as well. Propagation speed differed only slightly between the two forecasts, allowing the differences in intensification to be explored through height tendency differences between the two forecasts. Model results show that at 500 mb, latent heat release affects the height tendencies primarily through indirect means, chiefly by enhancing vorticity advection. Differential thermal advection and vertical advection of static stability tended to offset each other, as did vertical advection of vorticity and tilting effects. A height anomaly due to latent heat release was located downstream of the 500 mb trough and served as a focus for forcing differences associated with latent heating.

TABLE OF CONTENTS

I. INTRODUCTION 1

II. BACKGROUND 4

III. SYNOPTIC DISCUSSION 14

A. DISCUSSION OF ANALYSES 15

1. 1200 UTC 18 January Analyses 15

2. 1200 UTC 19 January Analyses 15

3. 0000 UTC 20 January Analyses 17

4. 1200 UTC 20 January Analyses 20

B. PERFORMANCE OF THE NGM 22

C. FORECASTS WITH AND WITHOUT LATENT HEAT RELEASE . 28

IV. COMPUTATIONAL TECHNIQUES 33

V. RESULTS 36

A. 24 h FORECAST 37

B. 36 h FORECAST 47

C. 48 h FORECAST 55

VI. CONCLUSIONS 67

A. DISCUSSION AND CONCLUSIONS 67

B. RECOMMENDATIONS 69

APPENDIX: THE NESTED GRID MODEL (NGM) 71

REFERENCES 73

VII. INITIAL DISTRIBUTION LIST 77

LIST OF FIGURES

Figure 1. NGM analyses, 12Z/18 16

Figure 2. As in Fig. 1, except 12Z/19 17

Figure 3. Sanders' Analysis, 12Z/19 18

Figure 4. As in Fig. 2, except 00Z/20 19

Figure 5. As in Fig. 3, except 00Z/20 20

Figure 6. As in Fig. 4, except 12Z/20 21

Figure 7. As in Fig. 5, except 12Z/20 22

Figure 8. NGM 24h forecasts, verification time 12Z/19 24

Figure 9. As in Fig. 8, except 36h forecast 25

Figure 10. As in Fig. 9, except 48h forecast 26

Figure 11. LHR vs. NLHR, 24h forecast 29

Figure 12. As in Fig. 11, except 36h forecast 30

Figure 13. As in Fig. 12, except 48 h Forecast 32

Figure 14. Computational Domain 35

Figure 15. 12 h Difference Fields at 500 mb 38

Figure 16. Total Height Tendency Fields at 500 mb, 24 h forecast 39

Figure 17. As in Fig. 16, except ZADV 41

Figure 18. Relative Vorticity at 500 mb, 24 h forecast 42

Figure 19. Absolute Vorticity Advection multiplied by f (ZADV) at 500 mb, 24 h forecast 43

Figure 20. As in Fig. 16, except for DTAD 44

Figure 21. Differential thermal advection at 500 mb, 24 h forecast 45

Figure 22. As in Fig. 20, except for DSIG 46

Figure 23. As in Fig. 22, except Total Height Tendency Fields, 36 h forecast 49

Figure 24. As in Fig. 23, except for ZADV 51

Figure 25. As in Fig. 18, except 36 h forecast 52

Figure 26. As in Fig. 24, except for DTAD 54

Figure 27. As in Fig. 26, except for DSIG 56

Figure 28. As in Fig. 27, except for Total Height Tendency Fields, 48 h Forecast 58

Figure 29. As in Fig. 28, except for ZADV 60

Figure 30. As in Fig. 25, except 48 h forecast 61

Figure 31. As in Fig. 18, except 48 h forecast 62

Figure 32. As in Fig. 29, except for DTAD 63

Figure 33. As in Fig. 32, except DSIG 64

Figure 34. DQTOT, DZET, and TILT Height and Height Tendency Difference Fields at 500 mb 65

I. INTRODUCTION

The study of latent heating effects on the development of extratropical cyclones has great precedent; several representative studies are outlined below and in Chapter II. Many of these studies focus on changes in storm intensity brought about by removing or varying latent heating in computer simulations. There is widespread agreement that latent heat release contributes to intensification, and in some cases is responsible for intensification. The present study is the direct descendant of two previous investigations into the effects of latent heat release using a diagnostic height tendency equation: Pauley and Smith (1988) and Tsou et al. (1987). While these studies have focused on continental cyclogenesis cases, this study applies the same techniques to a case of oceanic rapid cyclogenesis which shows a greater sensitivity to latent heating than previous continental cases.

Of particular interest in this study is the role of latent heat release in not only building the 500 mb ridge, but amplifying the trough as well. Dare and Smith (1984) used the Drexel-NCAR Limited Area Mesoscale Prediction System (LAMPS) model to analyze the effects of latent heat release on a winter continental storm. Their results show latent heat release aided ridging, but did not amplify the trough. Chang et al. (1982) examined a spring continental cyclone also using the LAMPS model. Their results show latent heating effects deepened the trough by approximately 70 m, as well as enhancing ridging. Robertson and Smith (1983) used the LAMPS model to assess the

effects of latent heat release on the same storm examined by Chang et al., and on a winter continental storm, finding 60 m height falls in the 500 mb trough over 48 h in the latter case.

Pauley and Smith (1988) examined the role of latent heat release by using a diagnostic model based on the generalized height tendency equation to compare and contrast model runs with and without latent heat release effects. The storm under study was a continental winter storm whose central pressure deepened by 9 mb over 48 hrs, with most of the deepening occurring in the last 24 h. Pauley and Smith found that vorticity advection produced the largest height tendencies, followed closely by differential thermal advection and vertical advection of static stability. Differential heating, the direct effect of latent heat release, produced much smaller height tendencies at 500 mb. Since differences in the adiabatic terms accounted for much of the difference between Limited-area Fine-mesh Model (LFM) forecasts made with and without latent heat release, intensity was affected by what were termed indirect effects of latent heat release.

Tsou et al. (1987) conducted a similar series of experiments using the same diagnostic model. Height tendencies were computed based on objective analyses from a winter continental storm which deepened 20 mb in 48 h, again with most of the deepening occurring in the last 24 h. Tsou et al. found that throughout the troposphere, vorticity advection produced the largest height tendencies, followed by differential thermal advection, and vertical advection of static stability, which tended to offset other terms and slow development. Differential heating produced much smaller height

tendencies, although it was responsible for large height changes over limited areas in the lower atmosphere.

The present study, like the studies cited above, also uses the general height tendency equation to analyze model runs with and without latent heat release. Unlike the papers cited above, the subject of this study is an oceanic rapidly deepening cyclone which was not well predicted by operational forecast models and which showed great sensitivity to latent heat release. In fact, excluding latent heat release led to a surface cyclone which essentially did not deepen, and a 500 mb short-wave trough which weakened over time. This is contrasted with the 35 mb/24 h decrease in central pressure and the formation of a 500 mb closed low in the full physics simulation. The objective of this study is to detail the role of latent heat release in developing the upper-level trough associated with this oceanic rapidly deepening cyclone.

II. BACKGROUND

In an attempt to provide timely warnings to mariners, as well as to increase their understanding of the processes of cyclogenesis and cyclone development, many meteorologists have investigated rapidly deepening extratropical cyclones. These maritime cyclones are significant hazards to shipping, best exemplified by the 10 September 1978 storm which intensified from 1004 mb to 945 mb in 24 h. The resulting winds and high seas damaged the Queen Elizabeth II and sank the dragger Captain Cosmo (Gyakum 1983). Rapidly deepening cyclones develop over a period of hours, vice days in the polar front theory, and offer an opportunity to observe dramatic changes in the environment over limited time and space. Sanders and Gyakum (1980) cite Tor Bergeron with developing the defining criterion for a storm to be labeled a rapid deepener: a central pressure fall at sea level of 1 mb h^{-1} for 24 h for a storm at 60 ° north. Sanders and Gyakum geostrophically scaled this criterion to any latitude by multiplying Bergeron's rate by (sin ϕ/sin 60°).

Sanders and Gyakum (1980) and Roebber (1984) found that rapidly deepening cyclones occur primarily in the winter months, peaking in January in the northern hemisphere, and in geographically preferred areas: in the western Atlantic and Pacific oceans near the Gulf Stream and Kuroshio Current. Rapidly deepening cyclones are characterized by unusually low central pressures, strong winds and correspondingly high seas. Hadlock and Kreitzberg (1988) conducted climatological studies covering 104

winter storms from 1966-1987 which also confirmed this geographic preference for rapid development, although Hadlock and Kreitzberg used a 10 mb drop in central pressure in 6 h as a definition of a rapid deepener. Their results were used to guide the Experiment on Rapidly Intensifying Cyclones over the Atlantic (ERICA) field study, an Office of Naval Research sponsored effort.

The coincidence of these storms with a sharp thermal gradient in the ocean suggests that surface fluxes play an important role. Nuss and Anthes (1987) assert that surface fluxes can strongly affect cyclogenesis by enhancing low-level baroclinicity, mid-tropospheric static stability, and moisture supply. However, modeling studies by Kuo and Reed (1988), and Kuo and Low-Nam (1990) show surface fluxes to have little to no effect on rapid deepening.

Kuo and Reed (1988) analyzed an explosively deepening cyclone in the Eastern Pacific with nine variations of the PSU/NCAR model, testing sensitivity to surface fluxes, latent heat release, surface friction, precipitation parameterization, and grid spacing. Kuo and Reed found that surface fluxes had no significant impact on storm development and intensity. Kuo and Low-Nam (1990) expanded this work for nine explosively deepening Western Atlantic cyclones in the context of short-range forecasts using the PSU/NCAR model. Again, surface fluxes were found to have only a minor influence on intensification.

Kuo et al. (1991) moderated their position somewhat after conducting further numerical experiments with the PSU/NCAR model examining the effects of heat flux, moisture flux and time of initialization on seven explosively deepening storms. They

determined that surface fluxes do indeed have an effect on rapid cyclogenesis, but that the effect is more of preconditioning the environment, rather than directly contributing to explosive deepening. Model runs initialized at the start of rapid deepening showed no sensitivity to the presence or absence of surface fluxes, while model runs initialized 24 h before the start of rapid deepening were dramatically affected. When surface fluxes were included to precondition the storm for 24 h, then turned off at the start of rapid deepening, the storm deepened at nearly the continuous flux rate. Thus Kuo et al. concluded that early surface fluxes made the potential for rapid development possible, but played a small role in actual rapid deepenening.

Although some debate exists about the role of surface fluxes in rapid cyclogenesis, there is general agreement that latent heat release (LHR) plays a critical role. Both Kuo and Reed (1988) and Kuo and Low-Nam (1990) determined LHR to be a major factor in cyclone intensification. The Kuo and Low-Nam study of nine storms ranked precipitation parameterization as the most important physical factor contributing to accurate modelling of rapid deepening. Kuo and Low-Nam tested three types of precipitation parameterization: the Kuo scheme, an explicit physics scheme, and the Arakawa-Schubert scheme. The three schemes were compared to observed results, and to a "dry" run with no latent heat effects included. The dry scheme fared the poorest, with central pressure errors of nearly 18 mb, barely producing explosive deepening, and generating mean position errors of 342 km after 24 h. The moist schemes performed much better, underforecasting central pressure by 6-8 mb after 24 h with mean position errors of 140-150 km. The Kuo and Reed case study found that the exclusion of LHR

from the model halved the rate of intensification and yielded storms which propagated more slowly.

Kuo and Low-Nam (1990) also noted the effect of LHR had a strong case-to-case variation among storms. In some cases, removing LHR effects had a small influence on central pressure; one storm lacking LHR effects achieved 90% of the full physics central pressure. However, other cases showed great sensitivity to LHR; one storm deepened its central pressure to only 39% of the full physics central pressure when LHR was removed. Kuo and Low-Nam concluded that some storms were dynamically forced, while others were diabatically driven.

Many other studies (Anthes et al. 1982, Chang et al. 1982, Anthes et al. 1983, Chen et al. 1983, Orlanski and Katzfey 1987, Pauley and Smith 1988) point to LHR as having significant influence on storm intensity, wind speed, and propagation speed. Most of these studies show that model simulations without LHR generate cyclones with central sea-level pressures 5-10 mb higher than model simulations including LHR. Additionally, near-surface wind speeds average $5ms^{-1}$ slower in runs without LHR. Finally, removing LHR generally resulted in slower moving cyclones.

Given that LHR plays a significant role in the intensification of cyclones, a more precise explanation of the affect of LHR on intensification is required. As a layer of air is heated diabatically, it will expand, resulting in increased heights for isobaric surfaces above the level of maximum LHR, and decreased heights for surfaces below the level of maximum LHR, in accordance with the height tendency equation. Since LHR tends to occur over limited regions and does not alter the mean field significantly, these height

rises and falls are local perturbations which are accompanied by vorticity decreases and increases, respectively. The omega equation shows that diabatic heating enhances upward motion. By mass continuity, upward motion is accompanied by upper-level divergence and lower-level convergence and the implied ageostrophic motions. Since warmer air is less dense than cold air, a column of warm air will exert less pressure on the earth's surface than an equal volume of cold air. Hence, as a result of localized LHR, surface pressure drops, low-level vorticity and convergence increases, upper-level vorticity decreases, and upper-level divergence increases.

Uccellini (1990) cautions against assigning a percentage to LHR to describe its effect on intensification, since the LHR mechanism may work directly to decrease sea level pressure through hydrostatic processes or indirectly though baroclinic processes. Uccellini holds that dynamical and diabatic processes are linked in a rapid feedback loop, possibly producing nonlinear interactions.

Pauley and Smith (1988) examined direct and indirect effects of LHR on a synoptic-scale wave system. Limited-area Fine-mesh Model (LFM) runs were made with and without LHR. Pauley and Smith defined the direct influence of LHR in the context of a generalized height tendency equation; the direct forcing of the height field by LHR is contained in the diabatic term. Indirect forcing was determined by comparing the adiabatic terms in the equation as computed from forecasts with and without LHR. Pauley and Smith found that at and above 500 mb both indirect and direct affects were important, but that direct effects dominated below 500 mb. These findings agree with Tsou et al. (1987) who found that vorticity advection was the most important forcing

mechanism overall, especially in the upper troposphere, but that LHR was significant in specific geographic areas.

The recent history of the prediction of rapidly deepening cyclones is encouraging. Sanders and Gyakum (1980) examined forecast accuracy of the six- and seven-layer primitive equation (6-LPE and 7-LPE) models of the National Meteorological Center (NMC). The 6-LPE model forecasts generally predicted central pressure drops of only 25% of the analyzed deepening, while the 7-LPE model with gridpoint spacing half that of the 6-LPE model was able to forecast only 33% of the analyzed deepening. Sanders suggested that improvements in model physics would reap greater benefits than increases in grid resolution.

The LFM, a direct descendant of the 7-LPE, proved to be a major step forward in predicting rapid deepeners. The LFM 12-24 h forecast predicted 58% of the analyzed central pressure deepening in the mean, more than a 50% improvement over the 7-LPE (Sanders 1986). Sanders attributed the improvements to better horizontal resolution, better analyses, and better accounting for sea surface evaporation. Sanders also found that the LFM forecast storm tracks were slightly faster than actual storm tracks, with a 340 km error in the 48 h forecast.

The Nested Grid Model (NGM), as detailed in the Appendix, provided the next significant improvement to NMC operational forecast skill, particularly off the east coast of the United States. Sanders (1987) showed that the NGM underdeepened cyclones by an average of only 1 mb in the dense mesh C-grid area and 7 mb in the less dense B-grid/C-grid overlap area for the 12-24 h forecast. Sanders (1987) cited improved

analyses, better resolution, and better treatment of boundary-layer fluxes as contributing factors in improving forecast skill. Explosively deepening cyclones tend to occur offshore in a data-poor environment; degradation in the forecast and analysis of storms in these areas is therefore to be expected. Sanders suggests that initial data limitations are now the most important factor limiting prediction skill.

Although the NGM is a great improvement over previous operational models, the model does exhibit shortcomings. The NGM routinely underforecasts initial deepening of rapidly deepening cyclones, and then rapidly deepens developing storms in an attempt to catch up with analyzed central pressure. Usually, the model lags the storm, intensifying it past the actual time of maximum intensity (Sanders and Auciello 1989).

Forecasting the onset of explosive deepeners based solely on NGM forecasts is difficult since the model has demonstrable weaknesses in this area. To assist forecasters in predicting rapidly deepening cyclones, Sanders and Auciello (1989) developed a forecasting checklist in 1986. The checklist is designed to predict explosively deepening cyclones between 30-55°N and from the east coast of the U.S. out to 50°W, up to 36 h in advance. This checklist has been used at the National Weather Service Forecast Office in Boston for the past several winters.

The checklist is as follows:

1. Does a 500 mb absolute vorticity maximum of 17 x 10^{-5} s^{-1} or more exist in the NGM initial analysis in an area from 30-50°N and 85-110°W?

2. Does this maximum maintain initial intensity or strengthen on successive 12 h NGM forecast charts out to 48 h?

3. is this maximum forecast to move at an average of 30 kt or more through 48 h?

4. Does this maximum cross the East Coast between 32-45°N during the forecast interval?

5. Does a jet streak of 110 kt or greater exist at 250 or 300 mb within a 300 nm (550 km) radius in the semi-circle south of the initial vorticity maximum?

6. Does the NGM develop a surface low of 990 mb or deeper during the next 48 h over an area from 38-45°N and 55-75°W?

Answering yes to four or more of the above questions indicates a likelihood of rapidly deepening cyclogenesis. Item one in the checklist accounts for upper-level dynamic forcing upstream of a surface low. Item two ensures that the upper-level forcing is present in sufficient strength throughout the forecast period. Upper-level propagation speed, associated windspeed, wavelength, and vorticity advection are addressed by item three. Item four applies climatology, and implicitly accounts for the presence of coastal fronts, and the effect of the Gulf Stream on surface fluxes, preconditioning, and later LHR. Secondary circulations related to jet streaks, as well as cyclonic shear and upper-level divergence are addressed in item five. Finally, item six checks for the presence of a surface system to be enhanced by the above listed forcing mechanisms; Auciello (1991) stated that the NGM tends to develop weak cyclones off the east coast in response to upper level forcing. In summary, most of the checklist appears to be oriented toward dynamic forcing.

Sanders and Auciello (1989) report that for the winter of 87/88 the checklist predicted 12 out of 15 explosively deepening cyclones, with 6 false alarms. In the winter of 88/89, the checklist predicted 13 out of 16 explosively deepening cyclones,

with 7 false alarms. The NGM fares better than the checklist at the 12 to 24 h forecast time, but significantly worse for the 36 h forecast time, predicting explosively deepening cyclones only 35% of the time with a 20% false alarm rate at 36 h.

Since LHR has been found to be an important factor in explosive deepening, one might expect to see at least one checklist item devoted to LHR. Sanders and Auciello (1989) stated that the checklist was not meant to be all-inclusive, or even optimal. Another checklist item pertaining to LHR, with the aim of identifying which storms are sensitive to LHR effects, and consequently how LHR would effect the storm, could increase the checklist's success.

The problem of storms occurring in data poor areas was addressed directly by the ERICA field study. Conducted from December 1988 to February 1989, ERICA comprised data gathering by dedicated aircraft flying though storms, by drifting and moored buoys, and by all other conventional weather data gathering assets in the United States and Canada, including increased frequency of rawinsonde launches (Hadlock and Kreitzberg 1988). ERICA's three main objectives were to

1. understand the fundamental physical processes occurring in the atmosphere during rapid intensification of cyclones at sea,

2. determine those physical processes that need to be incorporated into dynamical prediction models through efficient parameterizations if necessary, and

3. identify measurable precursors that must be incorporated into the initial analysis for accurate and detailed operational model predictions.

This study addresses the above objectives by examining the role of LHR in a rapidly deepening ERICA storm. As discussed above, LHR release leads to intensification; this study will describe more precisely the role of LHR in intensification of this storm. Analyses based on ERICA data will be examined to determine the accuracy of NGM forecasts, and suggestions for improving forecasts will be made.

III. SYNOPTIC DISCUSSION

This section first will examine the NGM analyses covering the development of the ERICA IOP-5 storm, and compare them with Sanders' (1990) hand-drawn analyses, which incorporate all available in-situ surface data, including observations from ships, drifting buoys, ERICA aircraft, satellite imagery, and NMC weather charts to assess the precision of the NGM analyses. Next, NGM forecasts initialized at 12Z/18 will be compared to the NGM analyses to determine forecast accuracy; this forecast run, initialized 24 h prior to cyclogenesis, was chosen both to permit adequate model spinup before the period of interest, and to allow preconditioning of the maritime boundary layer by surface fluxes in view of Kuo et al.'s (1991) findings. Finally, this operational NGM forecast will be compared to one made withholding latent heating effects to consider the overall influence of LHR on the development of this cyclone.

The ERICA IOP-5 storm began development at about 1200 UTC 19 January 1989 (12Z/19) and quickly reached maximum intensity one day later at roughly 1200 UTC 20 January (12Z/20). Grell et al. (1991) report that the IOP-5 storm was chosen by forecasters as an example of a non-explosively deepening storm to contrast other ERICA IOP's. However, the central pressure of this cyclone fell 35 mb over the 24 h period, qualifying as a rapid deepener. This storm also propagated rapidly, with an average propagation speed of 24.7 ms^{-1} (48 kts) over the 24 h period.

A. DISCUSSION OF ANALYSES

1. 1200 UTC 18 January Analyses

At 12Z/18, 24 h before significant surface development began and the initialization time for forecasts examined in this thesis, the NGM's surface synoptic situation appeared relatively benign (Fig. 1 A). A 1005 mb low was centered near Green Bay, but the low from which the IOP-5 storm arose had not yet formed. Sanders' surface analysis for 18Z/18 (not shown) showed a weak pressure minimum off Cape Hatteras; it is this disturbance which was the incipient IOP-5 storm. The NGM surface analysis for 12Z/18 designates a low pressure area off Georgia. Since there are no closed isobars about the low, and since Sanders' analysis, based on more complete data, shows a low much farther north only 6 h later, the accuracy of the NGM low is suspect. On the 12Z/18 500 mb chart (Fig. 1 B), a trough extended from Minnesota through Iowa, Missouri and Kansas. An 18×10^{-5} s^{-1} absolute vorticity maximum was present over the Iowa/ Missouri border, due south of Des Moines. The positive vorticity advection (PVA) region associated with this trough was south of the existing surface cyclone and therefore not in a position to intensify this low.

2. 1200 UTC 19 January Analyses

Over the subsequent 24 h, the 500 mb trough propagated eastward, crossing the coast and intensifying the newly-formed low off Cape Hatteras. The NGM analysis (Fig. 2 A) showed that the incipient IOP-5 cyclone was located near 40°N,70°W, with a central pressure of 1005 mb. Thickness contours showed a slight "s-shape" to the

south and east of the Atlantic low, indicating significant warm and cold air advection and baroclinic wave amplification had started.

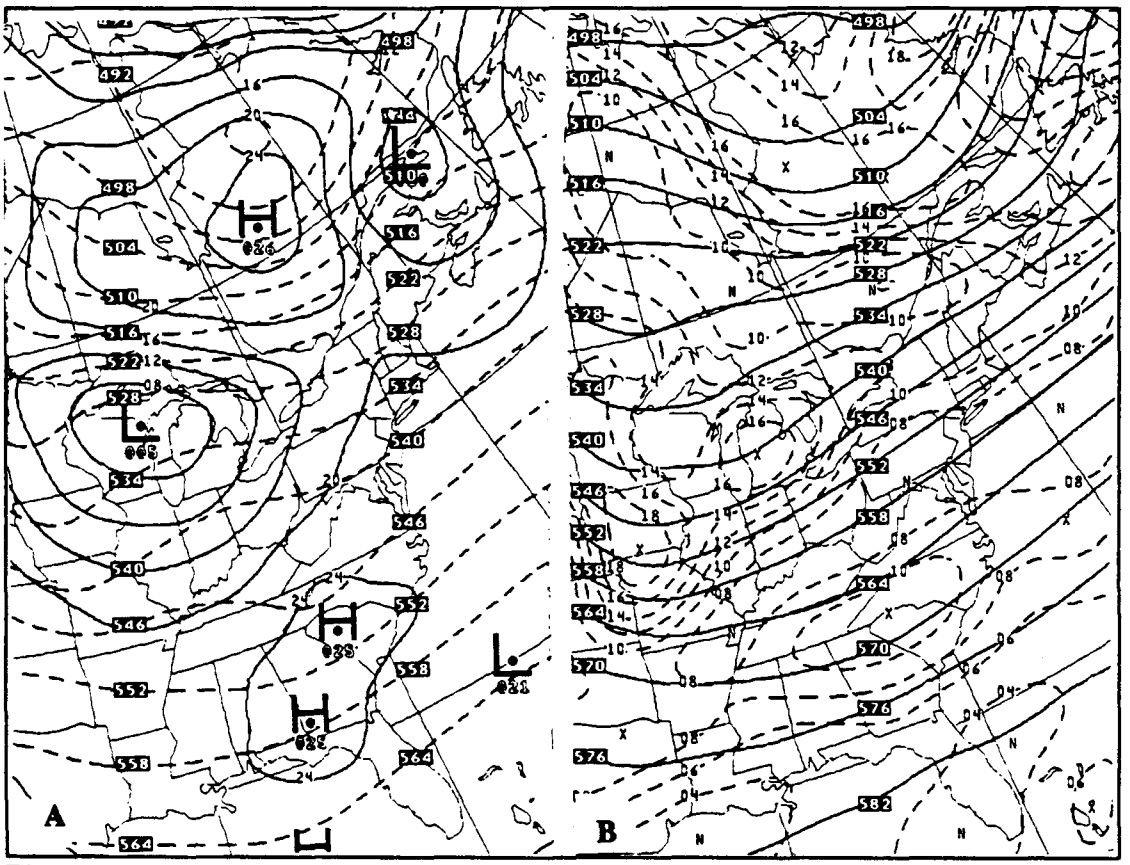

Figure 1. NGM analyses, 12Z/18: (A) sea level pressure, 4 mb increment, and 1000-500 mb thickness (dashed), 6 dm increment; (B) 500 mb heights 6 dm increment, and absolute vorticity (dashed), $2x10^{-5}$ s^{-1} increment

Sanders' analysis for this time (Fig. 3) agrees with the NGM analysis, with a 1002 mb low in the Atlantic slightly to the north and east of the NGM's position. Sanders' surface isotherms were still oriented SW-NE and well separated, indicating little surface frontogenesis.

Upper-level forcing is detailed by the NGM 500 mb analysis (Fig. 2 B). The trough in question moved from the Midwest to the Western Atlantic near 70°W. The

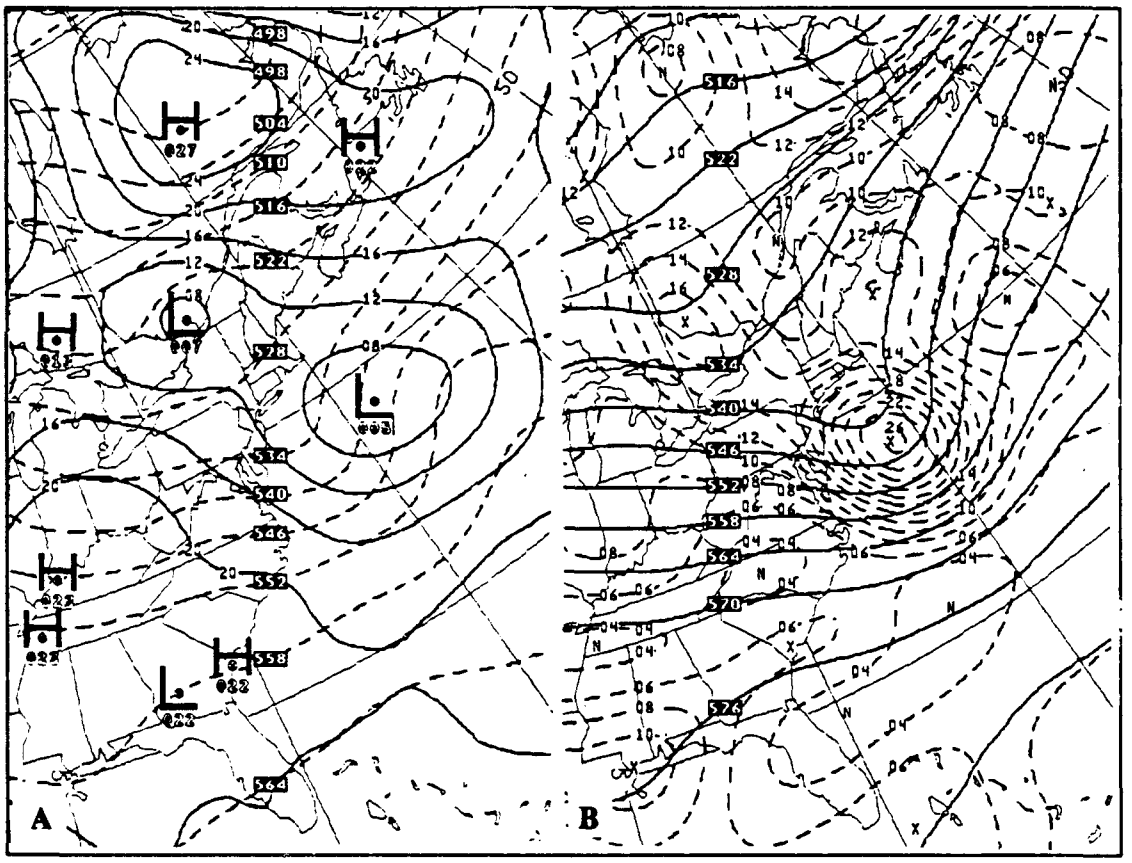

Figure 2. As in Fig. 1, except 12Z/19

absolute vorticity maximum intensified to 26×10^{-5} s^{-1} as the trough moved over a region of increasing cold air advection (CAA), associated with secondary cyclogenesis; a tight vorticity gradient developed as the wave amplitude increased. Strong upper-level PVA was analyzed over the surface cyclone's center, aiding in subsequent intensification. Slight ridging downstream of the trough was also evident; a 6×10^{-5} s^{-1} absolute vorticity minimum is associated with this nearly flat ridge.

3. 0000 UTC 20 January Analyses

By 00Z/20 the IOP-5 cyclone had intensified to 985 mb in the NGM analysis (Fig. 4 A). The cyclone propagated east to nearly 41°N 58°W, and had developed a

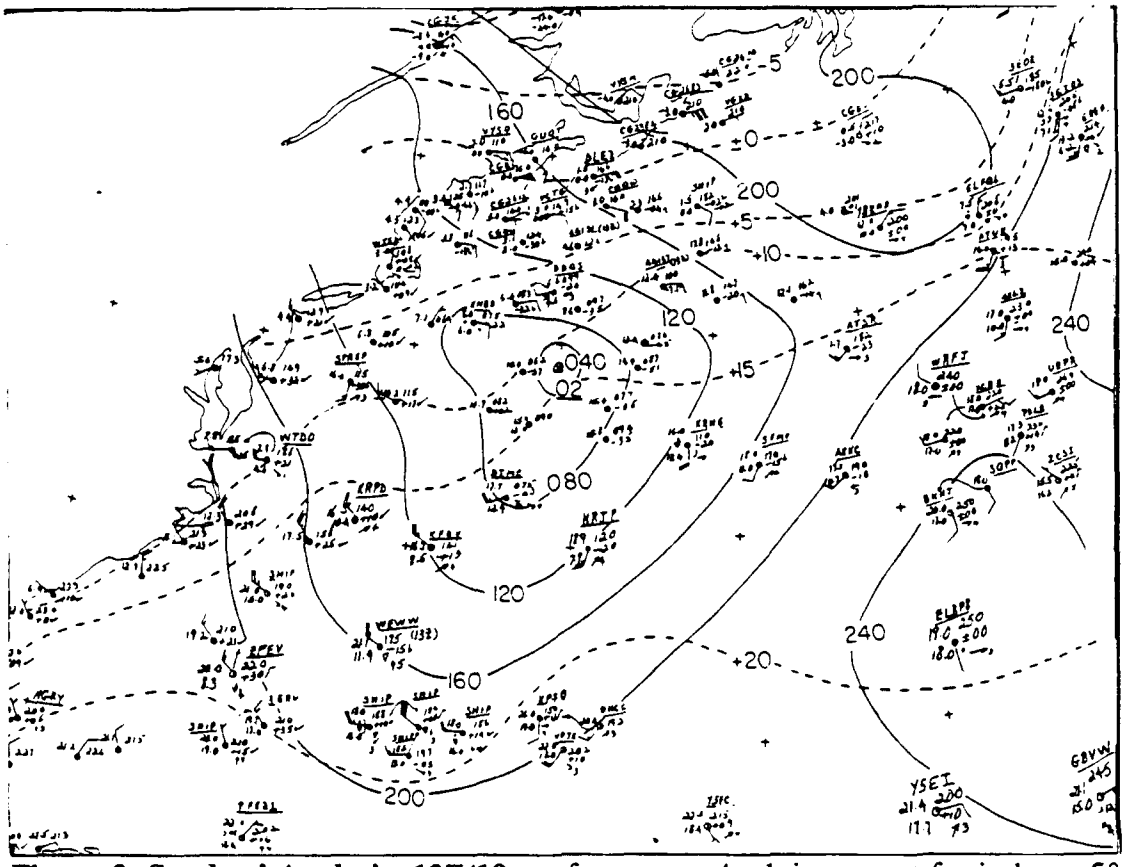

Figure 3. Sanders' Analysis, 12Z/19: surface press. 4 mb increment for isobars, 5° C increment for isotherms (dashed)

strong pressure gradient and strong thermal advection. Thickness contours had been distorted into a pronounced s-shape about the cyclone due to the strong low-level thickness advection.

The Sanders analysis (Fig. 5) is still in close agreement with the NGM analysis, with a 982 mb central pressure located farther west than the NGM cyclone center, but at the same latitude. The surface isotherms were more tightly packed along the warm front than the cold front, and took on more of a "s-shape" than 12 h earlier.

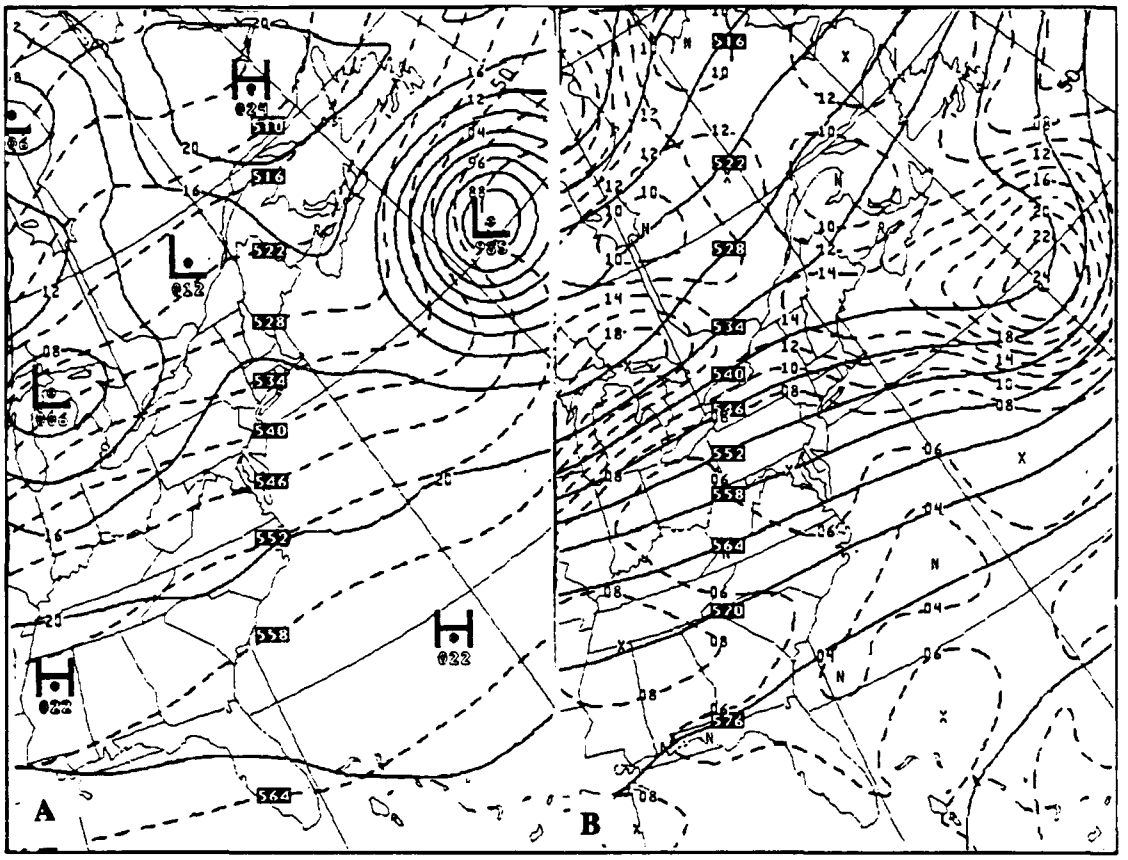

Figure 4. As in Fig. 2, except 00Z/20

At 500 mb (Fig. 4 B), the NGM analysis placed the trough at 60°W, just to the west of the surface low, and slightly decreased the absolute vorticity maximum to 24×10^{-5} s^{-1}. This decrease may be due to a paucity of observations over the ocean, rather than an actual decrease in intensity. Figure 4 B shows the trough over a region of CAA, an argument for intensification, not dissipation. Although the 500 mb trough was quite close to the surface low, PVA was still analyzed over the surface cyclone center, suggesting further intensification. WAA at the surface was helping to build the downstream ridge, which was especially noticeable along the 5400 m contour.

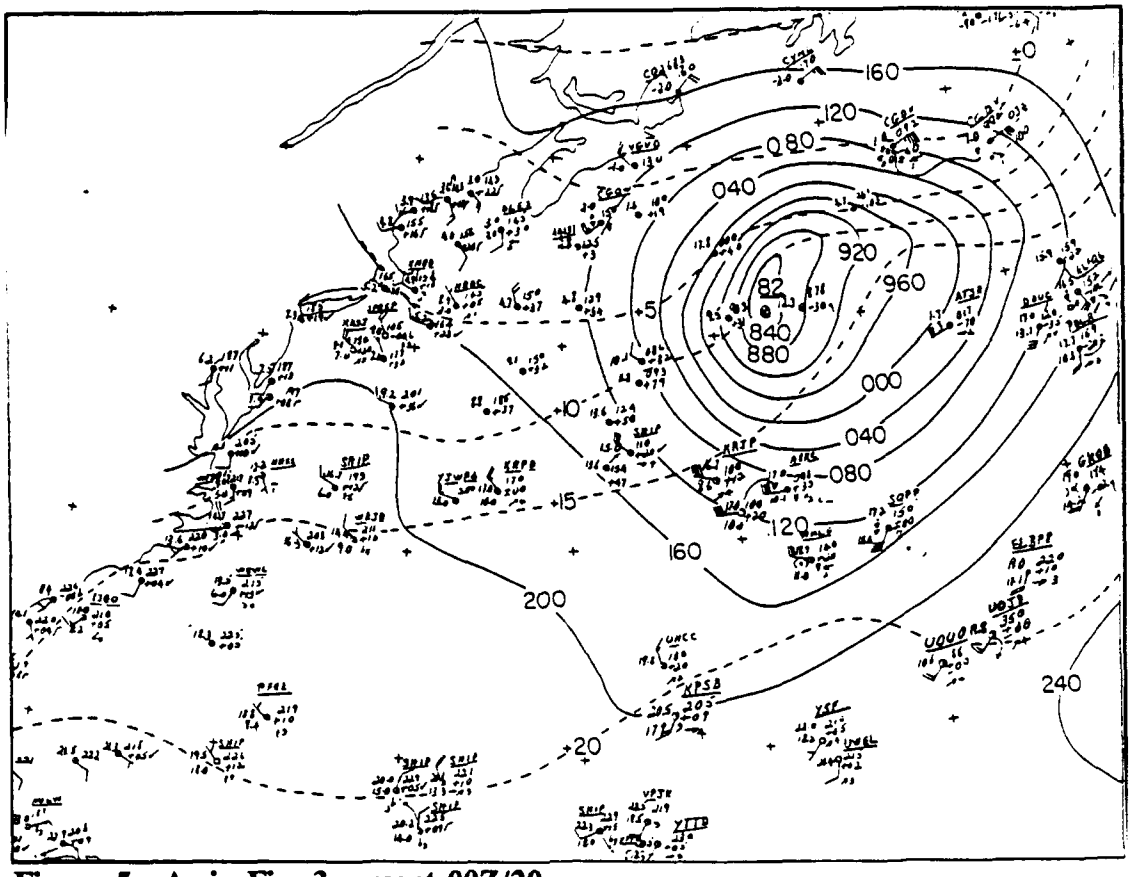

Figure 5. As in Fig. 3, except 00Z/20

4. 1200 UTC 20 January Analyses

The IOP-5 storm reached its maximum intensity at about 12Z/20. The center of the cyclone is not labeled on the NGM analysis (Fig. 6 A), but extrapolation from isobars indicates a central pressure of approximately 970 mb. The pressure gradient was strong, and thickness lines were packed along both the cold and warm fronts, indicative of advanced frontogenesis. Significant WAA was present, wrapping around the north side of the cyclone as the CAA edged along the south side. This thermal pattern helped to build the closed low aloft (Fig. 6 B).

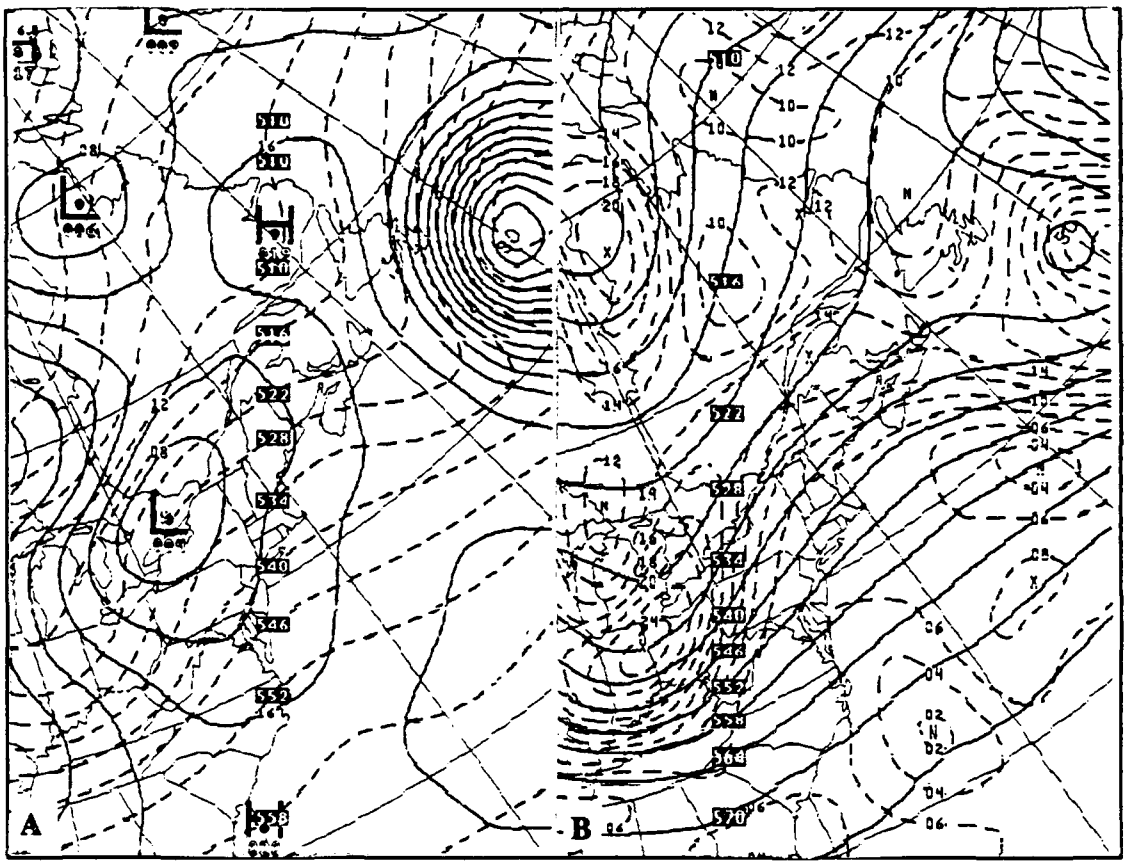

Figure 6. As in Fig. 4, except 12Z/20

Sanders' analysis (Fig. 7) concurs with the NGM, assigning a central pressure of 970 mb to the low and placing the cyclone center within a degree of the NGM analysis. The isotherms were again s-shaped and packed about the cold and warm fronts. Ship reports indicated winds over 25.7 ms^{-1} (50 kts) near the cyclone center.

The NGM 500 mb analysis (Fig. 6 B) showed a very high amplitude shortwave trough (over 10 degrees in latitude) with a closed low centered at 44°N 50°W. The system is vertically stacked, and therefore at the peak of intensity. The vorticity maximum is off the chart, but extrapolation from near-edge values indicates a maximum of at least $26x10^{-5}s^{-1}$.

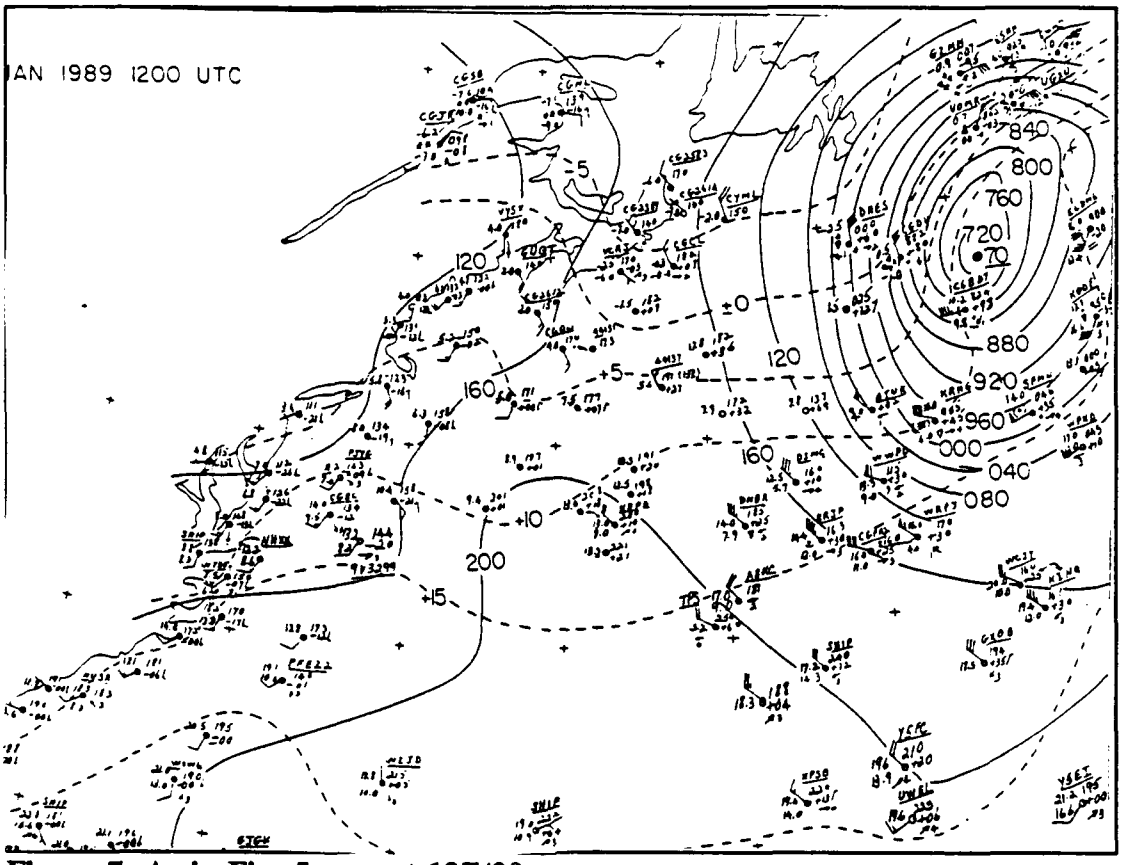

Figure 7. As in Fig. 5, except 12Z/20

B. PERFORMANCE OF THE NGM

Examining the NGM forecast charts and comparing them to the NGM analysis reveals a pattern of errors for the 12Z/18 forecast cycle. As discussed above, the NGM analysis charts correspond closely to Sanders' analysis charts; using the NGM analyses as "ground truth" for comparison of forecasts is reasonable.

The NGM 24 h surface forecast (Fig. 8 A) delayed forming the 1005 mb low over the Atlantic, instead elongating the low over Montreal. The failure to predict the

intensity of the secondary development seriously affected the NGM's forecast skill, and was a deficiency from which the NGM never completely recovered.

The 24 h 500 mb forecast (Fig. 8 B) predicts an $18x10^{-5}$ s^{-1} absolute vorticity maximum instead of the analyzed $26x10^{-5}$ s^{-1} maximum. Further, the forecast placed the trough west of the analyzed trough, away from surface CAA, lessening the effects of lower tropospheric forcing on the trough. The forecast $6x10^{-5}$ s^{-1} vorticity minimum is also slightly west of the analyzed minimum, but is in proper relation to the forecast trough.

The 36 h forecast (Fig. 9 A) made from the same initialization time (12Z 18 Jan) predicted a 994 mb low as compared to the 985 mb low in the analysis. The forecast low circulation was weaker than observed, with only four closed isobars, resulting in weaker CAA and WAA. The forecast surface cyclone still retained some of the elongation present in the 24 h forecast. Again, the forecast cyclone lagged the analyzed low, and was placed slightly to its north.

At 500 mb, the 36 h forecast (Fig. 9 B) trough was again too weak and lagged the analyzed system. The forecast trough had a much smaller amplitude, with less ridge building downstream, again due to weaker interaction between the low-level and upper-level features. Further, the forecast trough axis is oriented northeast/southwest, while the analyzed trough was oriented north/south.

The 48 h forecast (Fig. 10 A) showed an oblong 988 mb low oriented east/west, as compared to the tightly concentric deeper analyzed low. The forecast low again has four closed isobars, while the analyzed low had a tight gradient of 11 closed isobars.

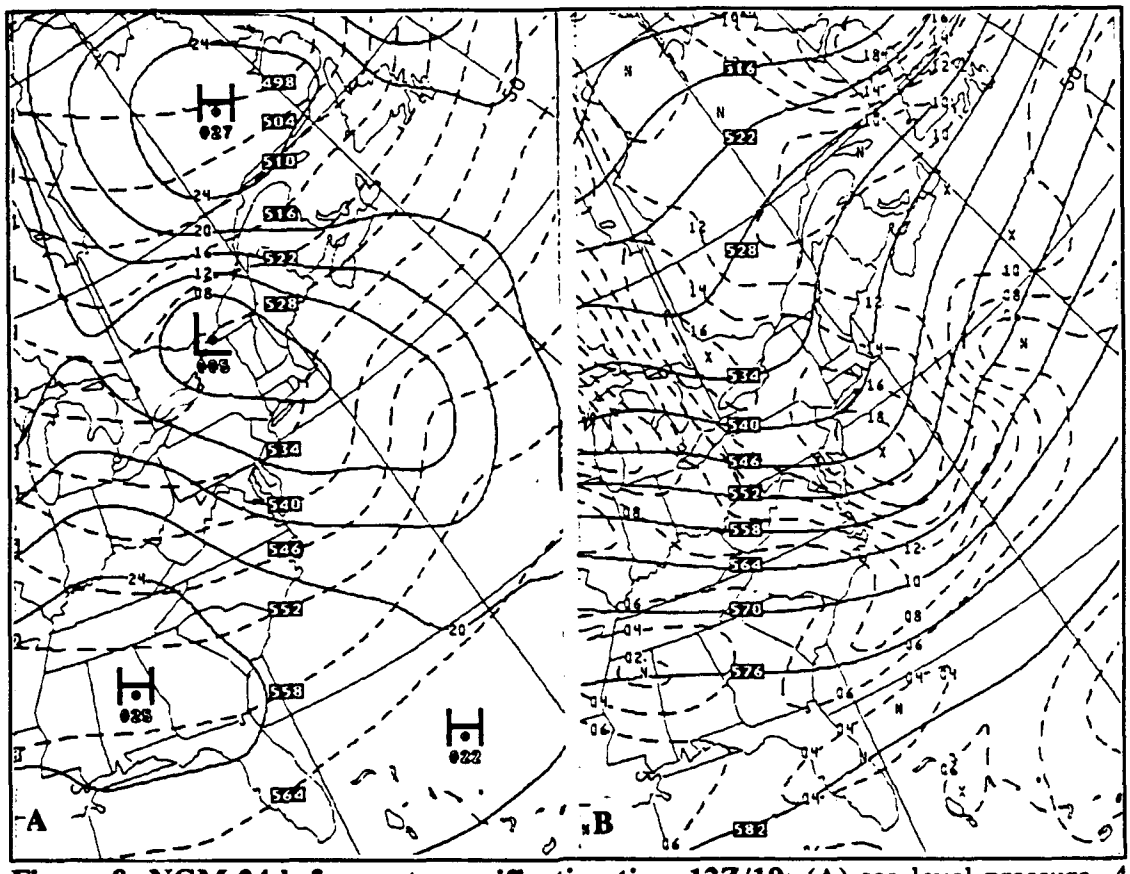

Figure 8. NGM 24 h forecasts, verification time 12Z/19: (A) sea level pressure, 4 mb increment, and 1000-500 mb thickness (dashed), 6 dm increment; (B) 500 mb heights 6 dm increment, and absolute vorticity (dashed), $2x10^{-5}$ s^{-1} increment

The forecast 500 mb trough (Fig. 10 B) developed a closed low aloft, as did the analysis, but was considerably weaker than the analyzed trough. The forecast 500 mb low lagged the analyzed low by approximately 5 degrees in longitude and was slightly north. The forecast produced some downstream ridge-building, but not the very intense ridging found in the analysis.

In general, the NGM underforecasts the initial development of explosively deepening maritime cyclones, and then rapidly decreases central pressure in an attempt

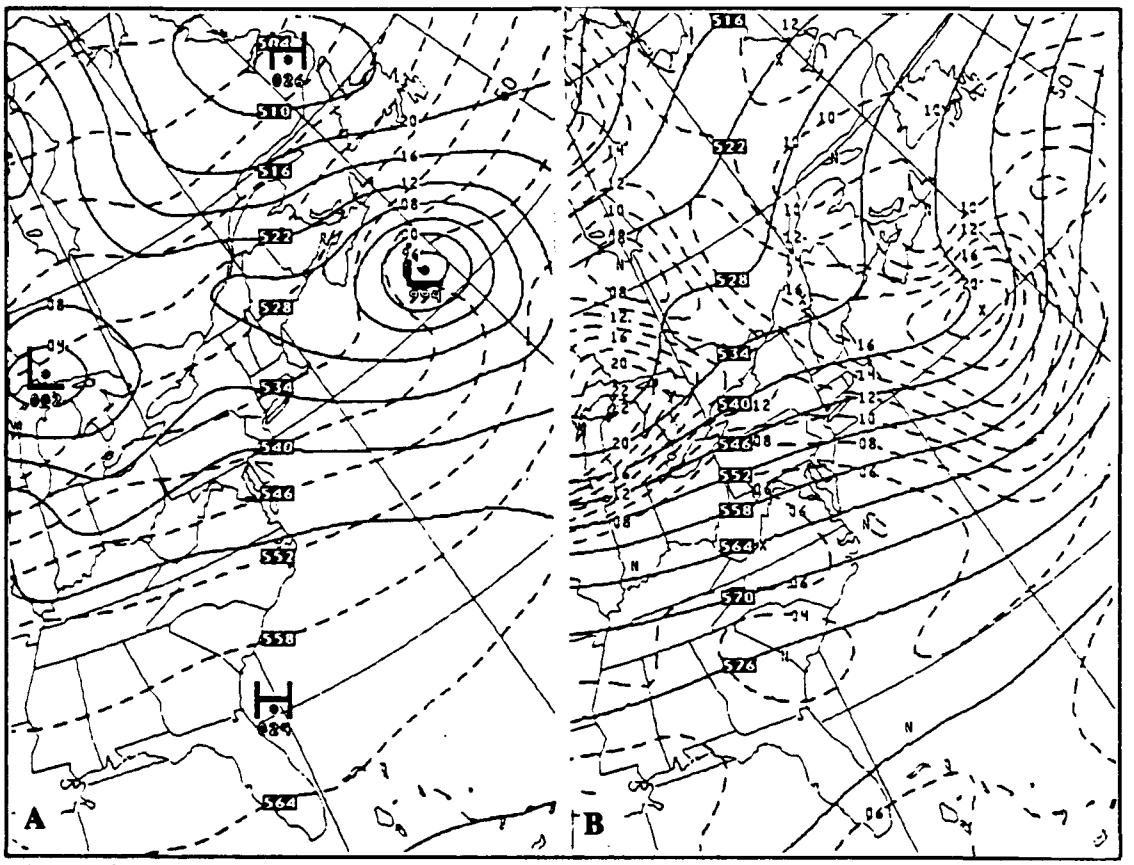

Figure 9. As in Fig. 8, except 36h forecast

to catch up with the analyzed central pressure. As a result, the model usually lags the storm (Sanders 1989), although the performance of the model is case dependent.

The NGM's inconsistency in forecasting rapid deepeners is demonstrated by a comparison of the model's performance for the ERICA IOP-4 and IOP-5 storms. IOP-4 was a primarily dynamically driven storm in which central pressure fell by 60 mb in 24 h; this storm was well forecast by the NGM. IOP-5 was a primarily diabatically driven cyclone which deepened by 35 mb in 24 h. It was poorly forecast by the NGM (Pauley et al. 1991).

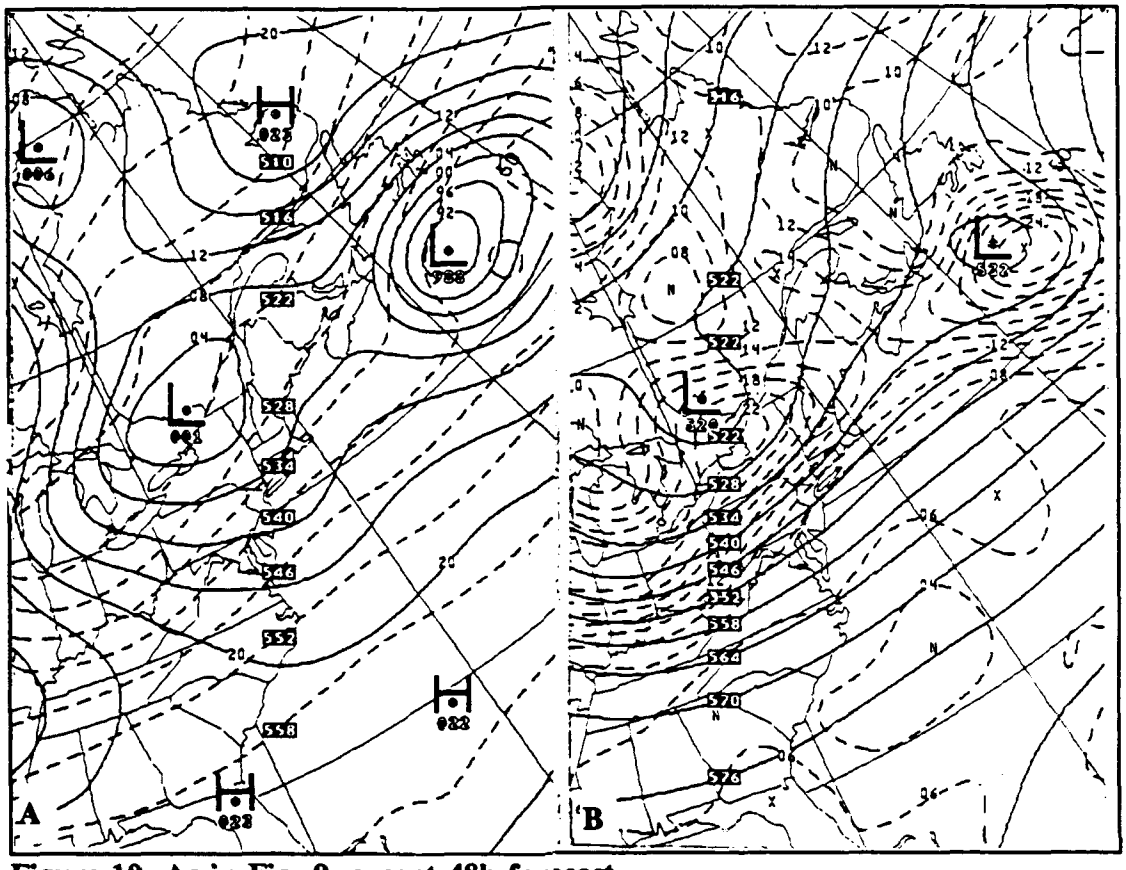

Figure 10. As in Fig. 9, except 48h forecast

At 12Z/19 Jan, 24 h before IOP-5 maximum intensity, the NGM analyzed the storm's central pressure as 1005 mb, and forecast it to drop to 982 mb, a decrease of only 23 mb in 24 h, barely qualifying as an explosively deepening cyclone. This 24 h forecast had an error of 12 mb, which is worse than the error of the 48 h forecast for IOP-4.

Throughout the development of the IOP-4 storm, the NGM displayed considerable skill. For at least 48 h before maximum intensity, the NGM accurately predicted the storm, forecasting central pressure to within 11 mb of the verifying NGM analysis, and position to within 2 degrees. At 24 h before maximum intensity, when central pressure

was still 998 mb, the NGM forecast a 42 mb drop in central pressure over the next 24 h and a propagation speed of 19.6 ms^{-1} (38 kts). This compares favorably with the analyzed drop in pressure of 52 mb and 21.1 ms^{-1} (41 kts) propagation speed (Pauley et al. 1991).

Table 1 (Pauley et al. 1991) details the somewhat erratic trend in the NGM's forecasts for the IOP-5 storm.

TABLE 1. NGM FORECAST CENTRAL PRESSURE AND LOCATION ERROR FOR IOP-5

Forecast Valid 12Z/20 Jan	Pressure (mb)	Pressure Error (mb)	Location Error (km)
00 h	970	--	--
12 h	978	8	126.2
24 h	982	12	321.8
36 h	988	18	321.8
48 h	987	17	558.9

Obviously, the NGM's forecasts were considerably less skilled for this case. Whereas the NGM 12 h forecast central pressure equalled the analyzed central pressure for IOP-4, the 12 h forecast for IOP-5 was still 8 mb too high. Forecast locations for both IOP's had similar accuracy at the 12 h forecast time, but at the 48 h forecast time IOP-4 was within 3° of the analyzed position, while IOP-5 was within only 7°, or 558.9 km (420 nm).

C. FORECASTS WITH AND WITHOUT LATENT HEAT RELEASE

Although intensification followed along the classic Petterssen development model (Petterssen, 1956), the unexpected *rapid* deepening of the IOP-5 storm may be due to latent heating effects. An analysis of model output comprising runs with and without latent heat release (LHR) included helps to determine the role of LHR in deepening the IOP-5 storm. These runs were initialized at 12Z/18.

At the 24 h forecast time (12Z/19), the operational forecast (OPNL) (Fig. 11 A,B) and the no latent heat release (NLHR) model runs (Fig. 11 C,D) were quite similar, differing in small details only. The 12 h precipitation forecast (not shown) indicated light precipitation, with a maximum of 14 mm/ 12 h (0.55 in/12 h) just downstream of the trough. Both the OPNL and NLHR runs showed a 1006 mb closed isobar feature in the same geographic area with a 16×10^{-5} s^{-1} vorticity maximum aloft.

In the 36 h forecast, differences were readily apparent. The OPNL forecast (Fig. 12 A,B) showed a 994 mb low with a stronger pressure gradient. Isobars were nearly circular and concentric from the center of the low to 1004 mb, but still failed to equal the deeper analyzed 982 mb low. The 12 h precipitation forecast (not shown) indicated heavier precipitation than the 24 h forecast, with a maximum of 28 mm/ 12 h (1.12 in/12 h) just downstream of the trough; increased precipitation coincide with larger differences between the runs. At 500 mb, the vorticity maximum had increased to 20×10^{-5} s^{-1}. This increase is quite noticeable near the tight bend in the 5400 m line over the center of the low. The downstream ridge was also building. In sharp contrast, the NLHR model run (Fig. 12 C,D) shows little to no development. Surface central pressure had dropped

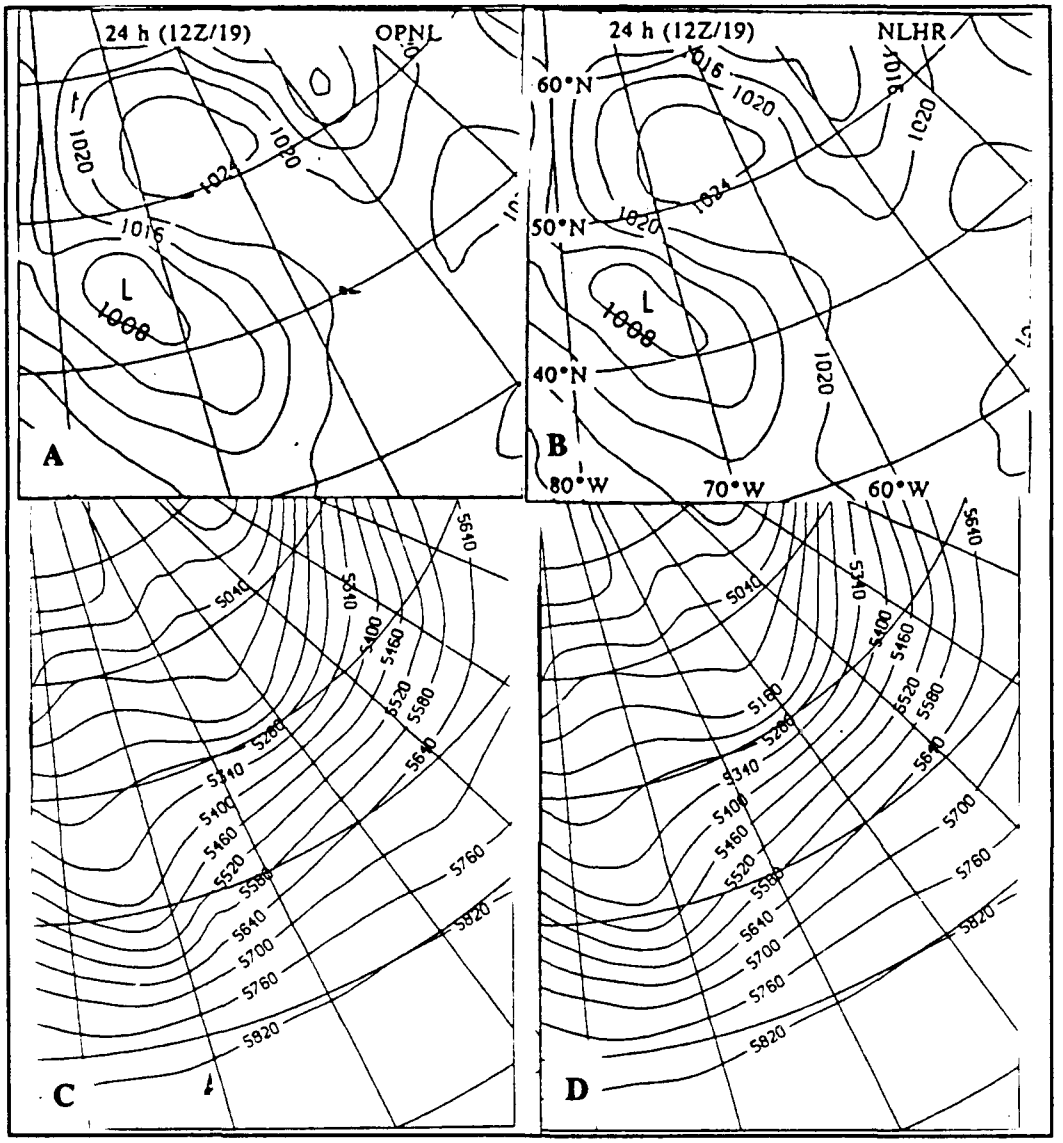

Figure 11. LHR vs. NLHR, 24 h Forecast: (A) OPNL run sea level pressure, 4 mb increment; (B) NLHR run sea level pressure, 4 mb increment; (C) OPNL 500 mb heights, 6 dm increment; (D) NLHR 500 mb heights, 6 dm increment

from 1006 to only 1004 mb. The gradient was much weaker than the operational forecast run, and the isobars retained their original oblong shape. The trough aloft had propagated but not intensified. There is no evidence of significant ridge building downstream, as the height contours appear rather flat.

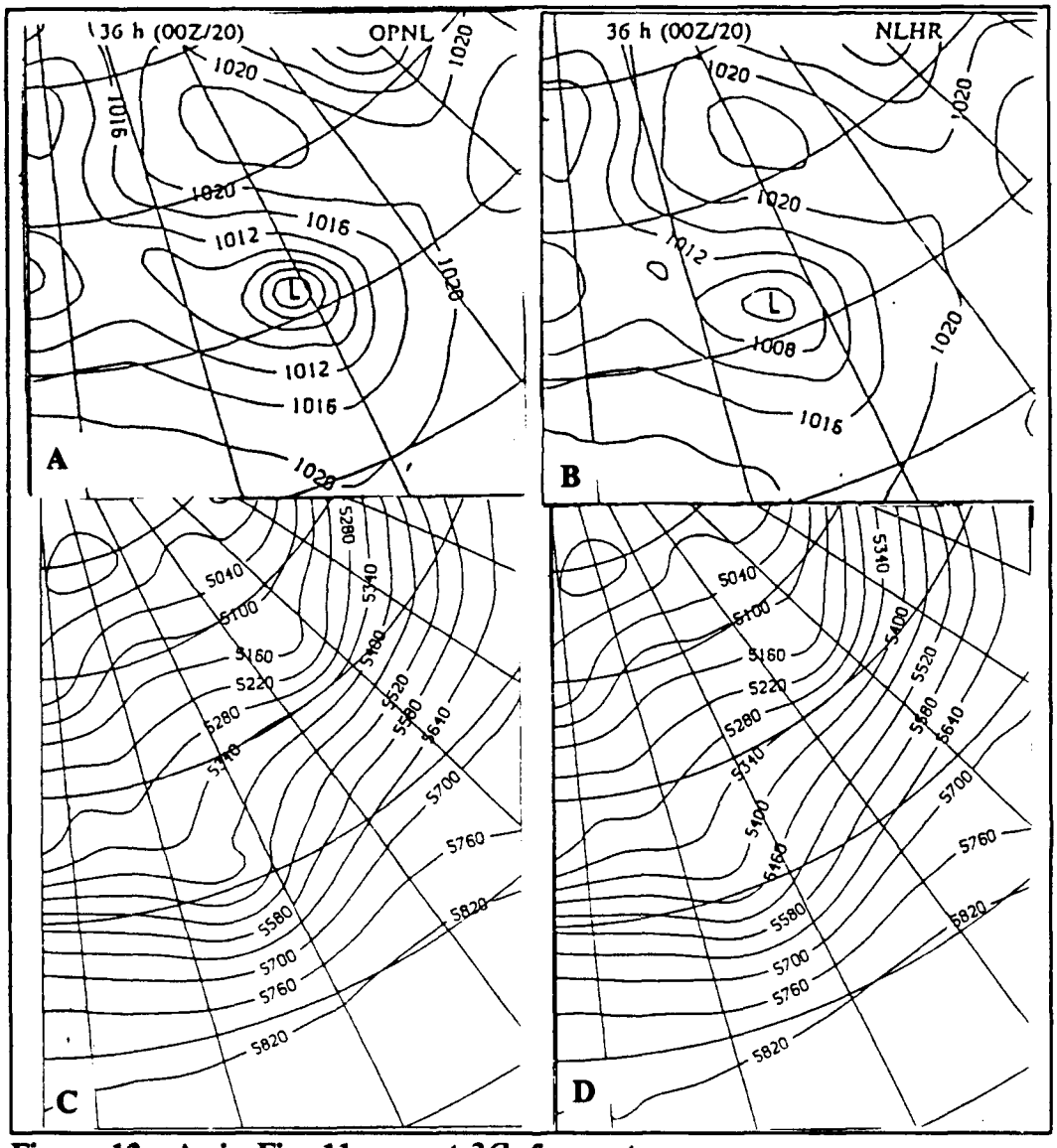

Figure 12. As in Fig. 11, except 36h forecast

Many of the contour lines are virtually identical in the two runs over large regions in the 24 and 36 h forecasts. Importantly, the most significant changes are found on a relatively small scale near the center of the storm, precisely where one might expect localized phenomena such as latent heat release to play a role.

By the 48 h forecast time, the two runs are considerably different. The OPNL forecast (Fig. 13 A,B) predicts a low with a central pressure of 988mb, while the NLHR run (Fig. 13 C,D) predicts a central pressure of 1004 mb -- no change from the 36 h forecast time, and a drop of only 2 mb in 24 h. The no latent heat run also slightly lags the OPNL forecast in propagation speed. Recall that the observed cyclone deepened to 970 mb, so even the OPNL forecast was deficient in the forecasting of IOP-5 deepening.

The OPNL run shows a closed low at 500 mb coincident with a 24×10^{-5} s^{-1} vorticity maximum. The closed low appears to have spun off the 5400 m contour, a reasonable progression considering the sharp bending of the line in the 36 h forecast field. The downstream ridge is well developed, with significant amplitude. On the other hand, the NLHR run shows some development of the trough and slight ridge building, but does not come close to predicting the closed low of the operational forecast.

In summary, the OPNL run develops an intensifying and rapidly propagating cyclone, while the NLHR run produces negligible intensification and slightly slower propagation. These findings are in accord with previous studies (Anthes et al. 1982, Chang et al. 1984, Anthes et al. 1983, Chen et al. 1983, Orlanski and Katzfey 1987, Pauley and Smith 1988) as discussed in Chapter II. However, the profound differences in the development of the upper-level trough have not been previously documented and so are the subject of this investigation.

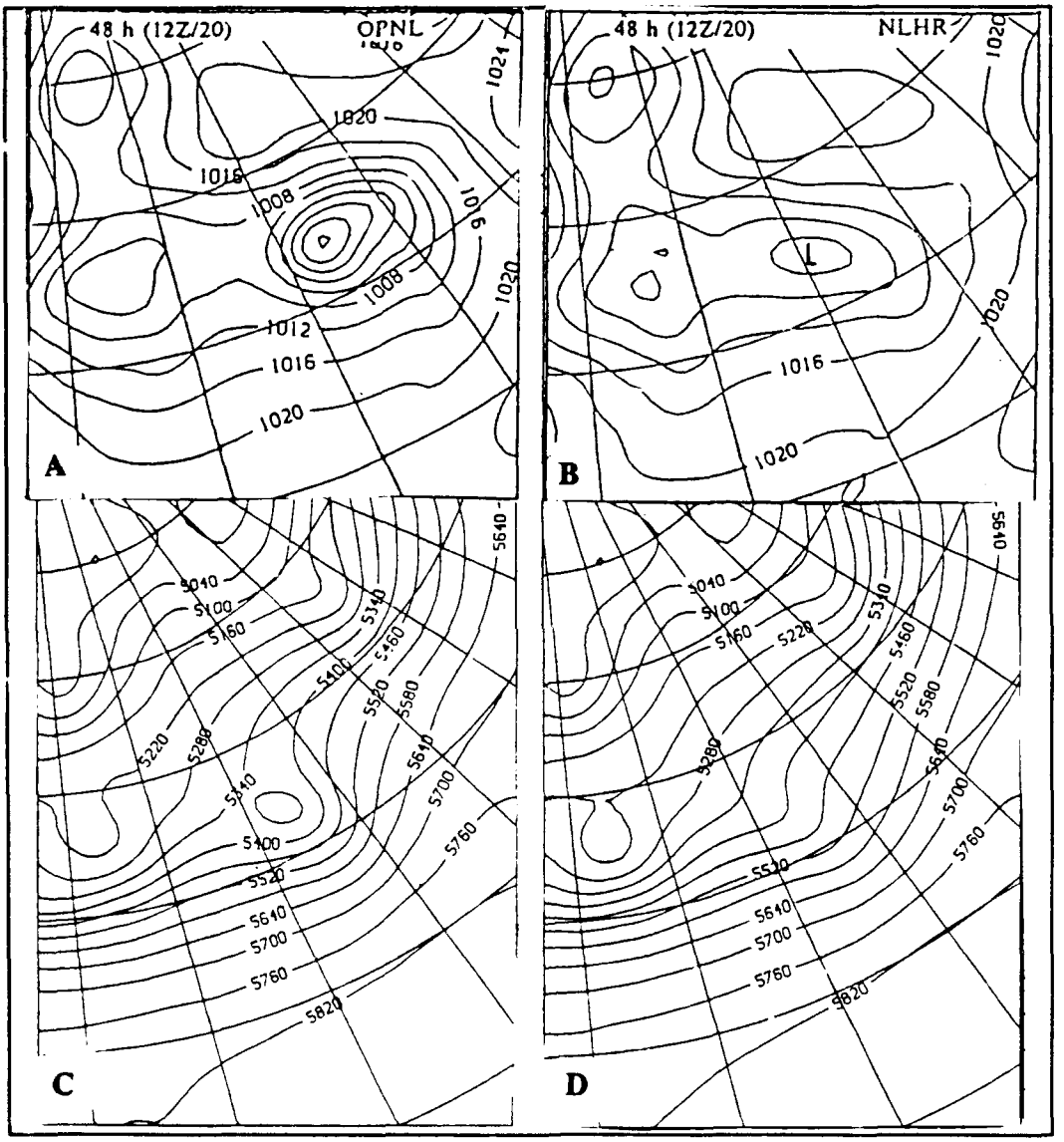

Figure 13. As in Fig. 12, except 48 h Forecast

IV. COMPUTATIONAL TECHNIQUES

The generalized height tendency equation (Tsou et al. 1987) provides the framework for the examination of the development of the upper-level short-wave trough. Derived from the thermodynamic and vorticity equations by assuming hydrostatic balance only, the generalized height tendency equation is given by

$$(m^2\nabla^2 + \frac{(\zeta + f)f}{\sigma}\frac{\partial^2}{\partial p^2})\frac{\partial \phi}{\partial t} - \frac{m^2}{f}\nabla f \cdot \nabla\frac{\partial \phi}{\partial t} + f\frac{\partial \zeta_{ag}}{\partial t} = -fm^2\frac{\vec{V}}{m}\cdot\nabla(\zeta + f)$$

$$(DELSQ) \qquad (BETA) \quad (TEND) \qquad (ZADV)$$

$$+ \frac{(\zeta + f)fm^2}{\sigma}R\frac{\partial}{\partial p}(\frac{\vec{V}}{m}\cdot\nabla\frac{T}{p}) - \frac{(\zeta + f)f}{\sigma}\frac{R}{c_p}\frac{\partial}{\partial p}(\frac{q}{p}) - \frac{(\zeta + f)f\omega}{\sigma}\frac{\partial \sigma}{\partial p}$$

$$(DTAD) \qquad (DQTOT) \qquad (DSIG)$$

$$- fm^2(\frac{\partial \omega}{\partial x}\frac{\partial}{\partial p}(\frac{v}{m}) - \frac{\partial \omega}{\partial y}\frac{\partial}{\partial p}(\frac{u}{m})) - f\omega\frac{\partial \zeta}{\partial p} + f\hat{k}\cdot\nabla X\vec{F}\ ,$$

$$(TILT) \qquad (DZET) \quad (FRICT)$$

where the variables take their usual meanings. The map factor m is used to account for the fact that a two-dimensional grid is projected onto a sphere; lines in the x and y directions are not coincident with latitude and longitude. Therefore, motion in the x direction, or u, produces north/south wind components as well as the expected east/west components. Similarly, the velocity component v has east/west as well as north/south components. The beta (BETA), ageostrophic vorticity tendency (TEND), and the friction (FRICT) terms in this equation are neglected as in Tsou et al. (1987).

Values for the variables in the height tendency equation are obtained from the NGM output on a 50 by 70 gridpoint subset of the innermost C grid, covering a region from southern Florida northward to Greenland, and from the Appalachians eastward to about 30°W (Fig. 14). The forecast grid system is rotated 20 degrees to the east of the operational configuration to ensure complete coverage of the IOP-5 storm area and to minimize boundary effects. NGM output values used are temperature, horizontal wind components, pressure surface height, vertical motion, specific humidity, and model predicted parameterized values of grid-scale and subgrid-scale latent heat release (LHR). Gridpoint spacing is 91.452 km at 60° north. Post-processing of NGM output converts sigma to pressure coordinates by interpolating linearly in the logarithm of pressure, resulting in a 19 level grid with pressure levels from 1000 to 100 mb in 50 mb increments. Since the NGM uses a staggered grid, post-processing also interpolates all values to all gridpoints; the resulting grid is therefore unstaggered. Smoothing is performed on all NGM model output values prior to calculations by using a low-pass fourth-order Shapiro filter (Shapiro 1975), which is mathematically equivalent to the smoother applied every half-hour during the forecast cycle in the NGM.

The forcing terms on the right-hand side of the equation are calculated independently, so that the solution by relaxation can be conducted using any or all forcing terms. Horizontal and vertical derivatives are calculated using second-order centered finite differences, except at the boundaries, where forward or backward differences are used as appropriate. After calculations are complete, the forcing terms are smoothed with a final pass of the Shapiro filter.

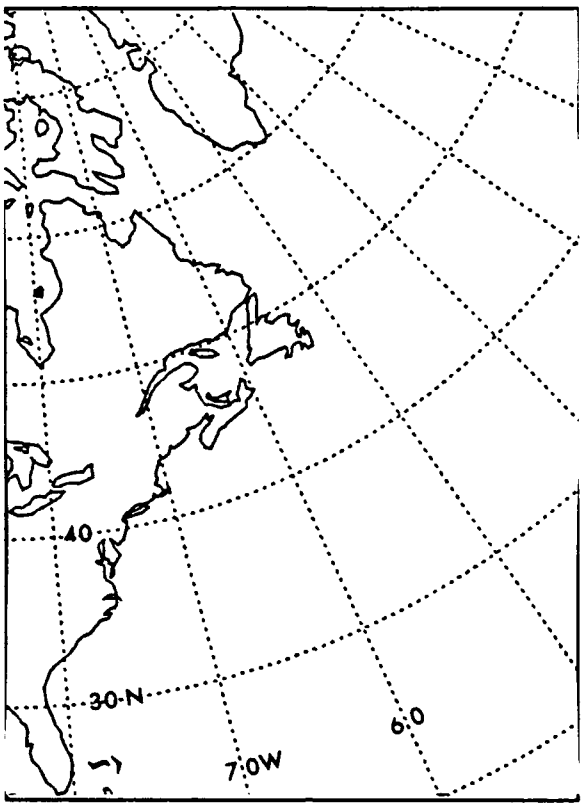

Figure 14. Computational Domain: 50x70 gridpoint region used in calculations

Since the equation is solved using elliptic methods, ellipticity must be maintained by ensuring that the coefficient $(f+\zeta)f/\sigma$ is positive. At points where absolute vorticity is negative or the lapse rate is near superadiabatic, the coefficient is set to $3x10^{-11}$ kg^2 m^{-4} s^{-4}, an arbitrarily small number. The height tendency is determined by successively over-relaxing either individual forcing terms or their sum. The convergence criterion is a maximum change in height tendency between iterations of less than $1x10^{-5}$ m^2s^{-2}; the over-relaxation coefficient is 1.5. Output height tendencies were scaled from m^2s^{-2} to m/12 h to facilitate comparison with finite difference height changes.

V. RESULTS

Using the procedures previously described in Chapter IV, height tendency solutions were determined for the linear combination of all six right-hand-side forcing terms, as well as each of the terms individually. These relaxation solutions yield instantaneous height tendencies valid at the synoptic times. To provide an accuracy check, the relaxation solutions were normalized to units of meters per 12 h and compared to simple height change fields (Figs. 15 A - D) generated by subtracting height fields bracketing the synoptic times by 6 h on either side. Comparing instantaneous tendencies to 12 h height change fields is not a perfect check, but provides some measure of verifying magnitude and location of important height tendency features. Specific comparisons of the 12 h height change fields with the instantaneous fields are found in the 24 h and 36 h forecast sections (the 48 h forecast is not compared since it is the final forecast time and cannot be bracketed by other forecasts). In general, there is close agreement on the location of the height falls/rises associated with the trough/ridge system, with rough agreement on magnitude. Finally, to aid in comparing the OPNL to the NLHR runs, the NLHR fields were subtracted from OPNL fields, resulting in difference fields of both heights and height tendencies. This has the added benefit of eliminating much of the height change due to propagation, since the OPNL and NLHR are moving at much the same speed, with NLHR lagging slightly. Using the height tendency fields, this section

will examine the effects of each of the terms in the height tendency equation on total height tendency over the 48 h period.

A. 24 h FORECAST

Height falls dominate the total height tendency pattern in both the OPNL and NLHR runs for the 24 h forecast (Fig. 16 A,B). Both runs show a height fall/rise pattern indicative of propagation, with height falls in the 500 mb trough, suggesting intensification. Since the height falls in the trough are greater in the OPNL run than the NLHR run, the OPNL forecast of the storm is expected to intensify more than the NLHR forecast. Both the OPNL and NLHR runs compare favorably to the 12 h height change fields (Fig. 15 A,B). Although the latter are more symmetric about the trough due to time averaging, the locations of prominent features and approximate magnitudes correlate well.

The 500 mb OPNL-NLHR height difference field (Fig. 16 C, heavy lines) shows a small difference in the downstream ridge, as the OPNL run builds its ridge and the NLHR does not. The resulting +20m difference (height anomaly) is located in the region of a small-scale bend in the 5520 m contour in the OPNL height field, which is absent in the NLHR field. Examining the OPNL 12 h precipitation forecast for 24 h (not shown) reveals a 13.97 mm/ 12 h (0.55 in/12 h) local maximum coincident with the height anomaly, providing evidence for the relationship between this feature and LHR. The height tendency differences (thin lines) are concentrated in the region just downstream of the trough. The negative values (dashed lines) indicate increased

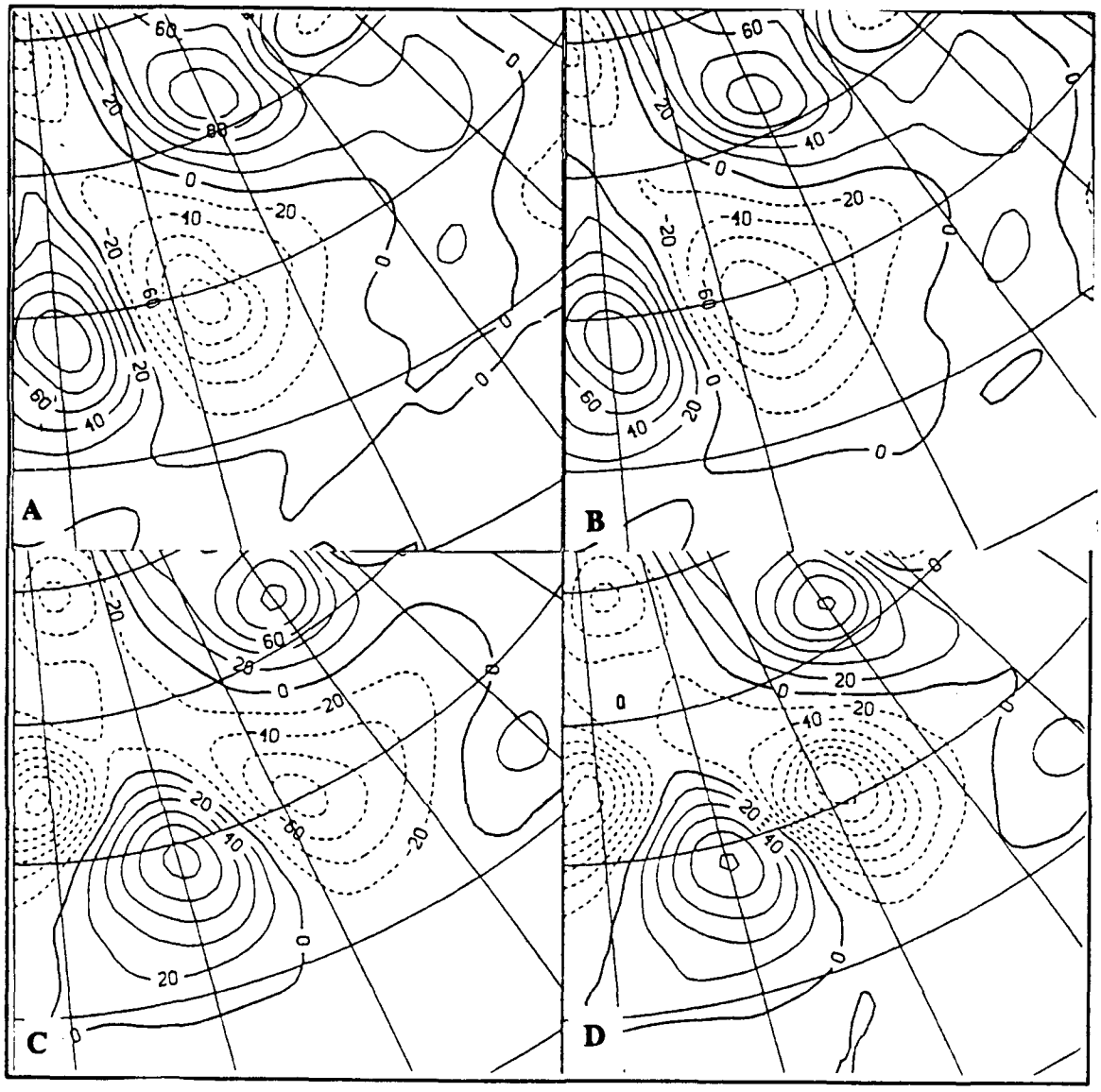

Figure 15. 12 h Difference Fields at 500 mb: (A) 24 h OPNL forecast, height tendencies (thin) 20 m/12 h increment; (B) 24 h NLHR forecast, heights and height tendencies; (C) 36 h OPNL forecast; (D) 36 h NLHR forecast

intensification in the OPNL, while positive values indicate increased ridge building in the OPNL run. It is important to note that almost all of the differences between the two fields occur downstream of the 500 mb trough: the area of LHR.

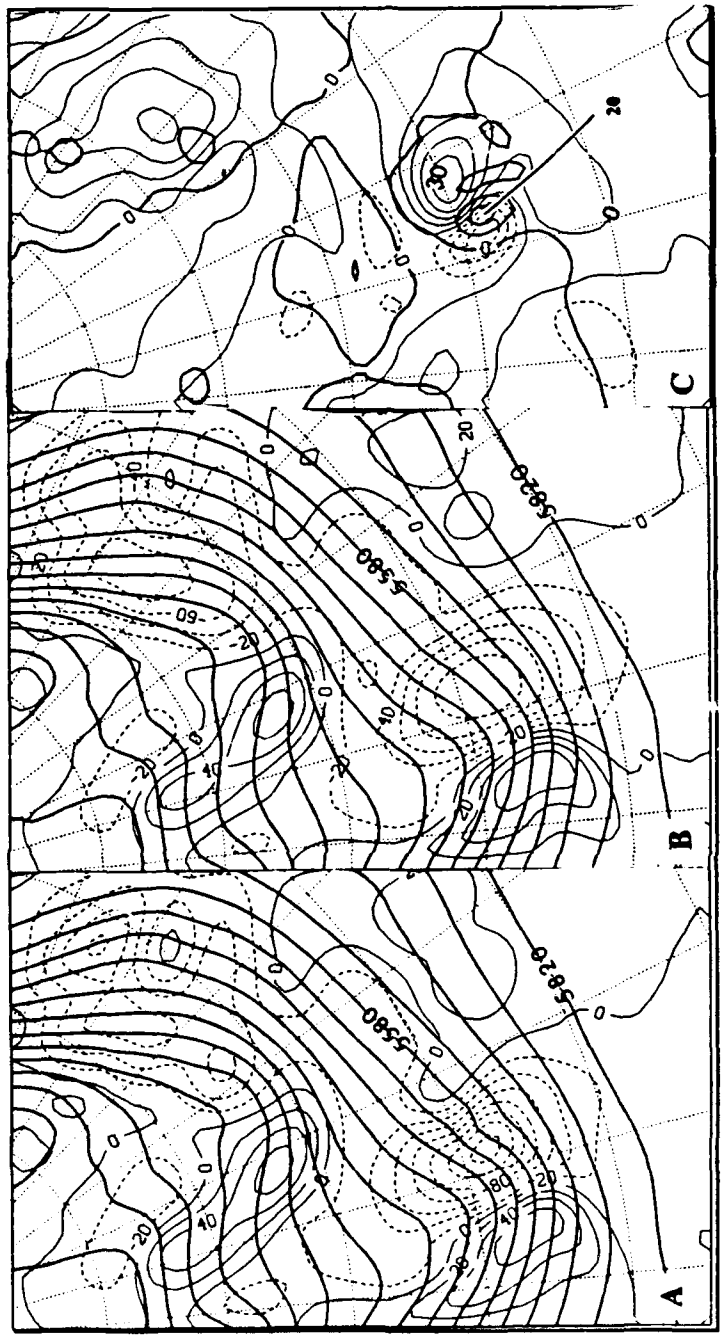

Figure 16. Total Height Tendency Fields at 500 mb, 24h forecast: (A) OPNL, heights (bold) 6 dm increment, and height tendencies (thin) 20 m/12 h increment; (B) NLHR, heights and height tendencies; (C) OPNL-NLHR Difference, height differences (bold) 1 dm increment, and height tendency differences (thin, dashed negative), 10 m/12 h increment

Examining the forcing terms individually offers insight into the precise role of LHR in enhancing the development of the upper-level wave. Vorticity advection (ZADV)

(Fig. 17 A,B) accounts for most of the total height tendency. The OPNL run (Fig. 17 A) shows height rises upstream of the 500 mb trough and height falls downstream of the 500 mb trough as expected, assuming a typical vorticity advection pattern. Height falls are much stronger than height rises, portending the propagation and intensification of the cyclone. Strongest height falls are associated with the height anomaly, as in the total height tendency pattern (Fig. 16 A). The NLHR run also shows the expected height rise/fall pattern, with height falls downstream of the trough weaker than those of the OPNL run. It is important to note that all ZADV height tendency differences between these two runs (Fig. 17 C) occur downstream of the trough, and that the largest differences occur in the region of the positive height anomaly, a result of the OPNL run having greater height falls than the NLHR run. A +20 m per 12 h height tendency difference appears farther downstream since the OPNL run has weaker height falls than the NLHR run downstream of the ridge axis.

Examining the forcing fields provides a dynamical explanation for the stronger height falls in the OPNL run. The height anomaly downstream of the OPNL 500 mb trough is associated with an area of strong relative anticyclonic vorticity (Fig. 18 A). (Relative vorticity is used because the vorticity advection differences in this case depend primarily on relative vorticity differences, and because relative vorticity differences are better delineated using the positive-solid-line negative-dashed-line scheme.) This increases the relative vorticity gradient in the OPNL run, as opposed to the NLHR run (Fig. 18 B), which lacks the height anomaly. The increased vorticity gradient results in increased absolute vorticity advection (Fig. 19 A,B) and therefore increased height falls.

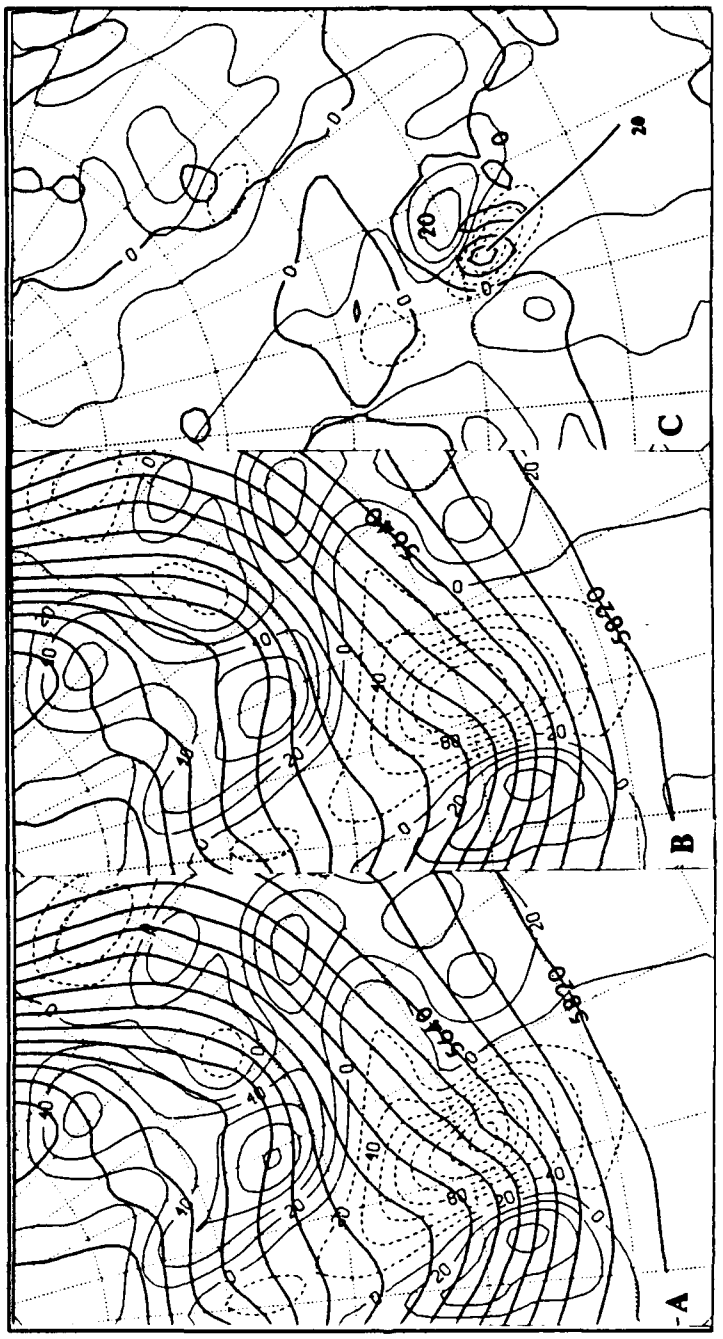

Figure 17. As in Fig. 16, except ZADV

The height tendencies associated with differential thermal advection (DTAD) are of roughly the same magnitude for the OPNL (Fig. 20 A) and NLHR (Fig. 20 B) runs,

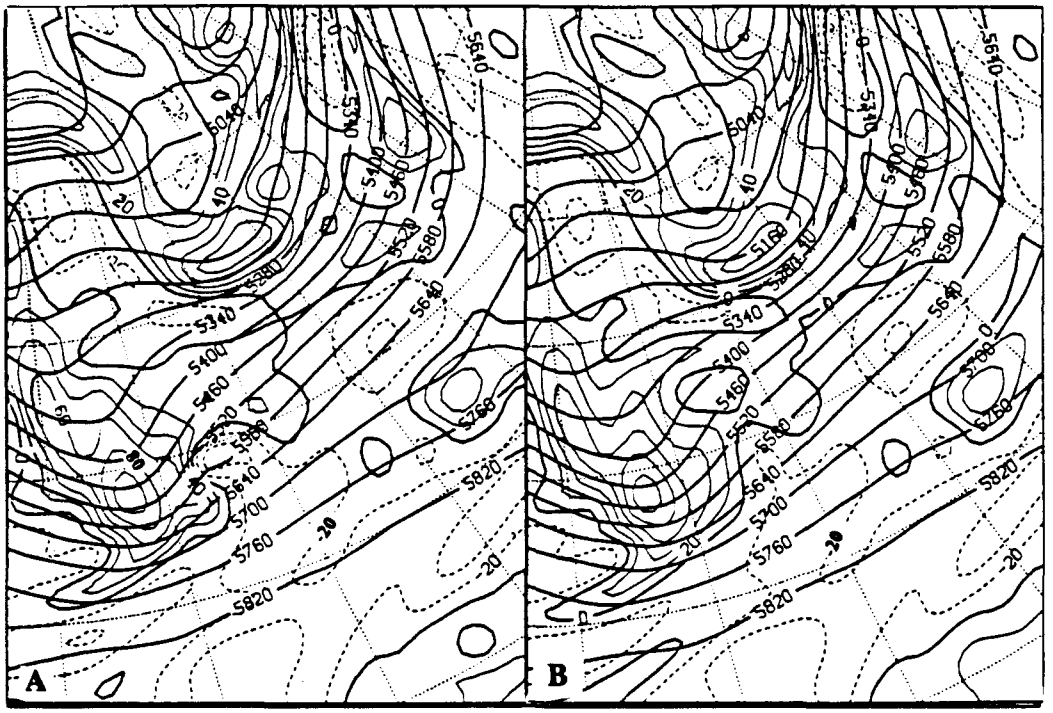

Figure 18. Relative Vorticity at 500 mb, 24 h forecast: (A) OPNL, heights (bold), 6 dm increment, and relative vorticity (thin, dashed negative), 20×10^{-6} s^{-1} increment; (B) NLHR

and nearly as large as the ZADV contribution. The DTAD height tendencies for both OPNL and NLHR runs show height falls downstream of the trough. This is the opposite of the expected result, since comparing the height fields from the 24 h and 36 h runs shows the downstream ridge to be building. Quasi-geostrophic theory attributes ridge building to warm air advection (WAA) decreasing with height and trough intensification to cold air advection (CAA) decreasing with height. This would lead one to expect to see height rises in the downstream ridge and height falls in the trough.

Examining the DTAD forcing fields (Fig. 21 A, B) shows positive forcing downstream of the trough, implying height falls, in both the OPNL and NLHR runs. The positive forcing is a result of warm air advection (WAA) increasing with height,

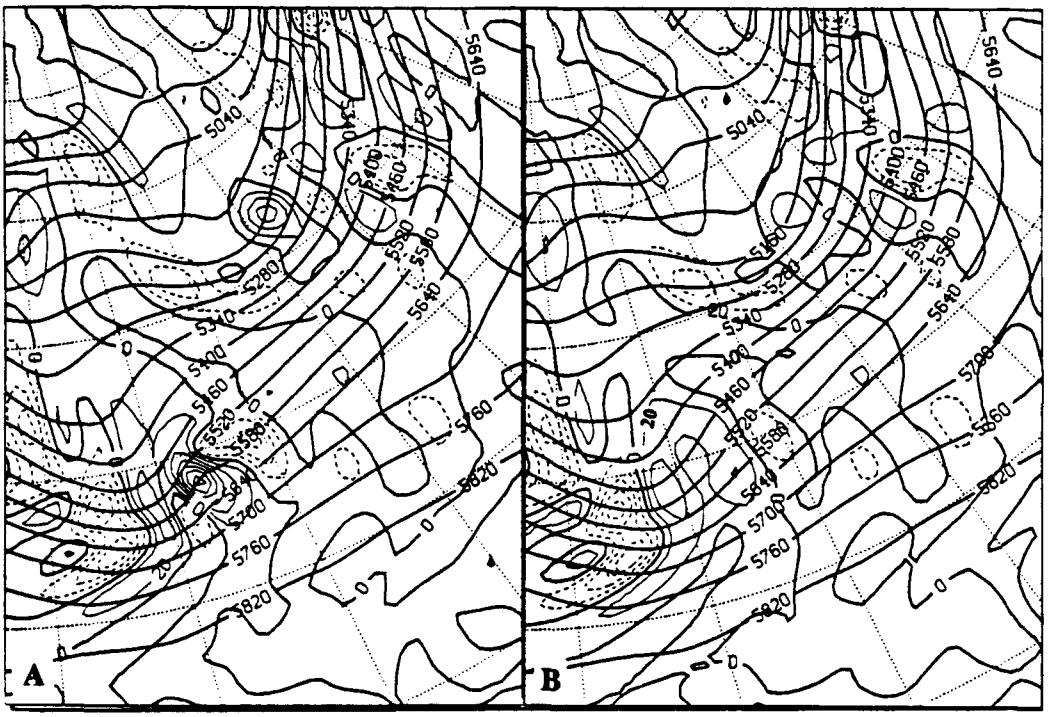

Figure 19. Absolute Vorticity Advection multiplied by f (ZADV) at 500 mb, 24 h forecast: (A) OPNL, heights (bold), 6 dm increment, and ZADV (thin, dashed negative), 20×10^{-14} s^{-3} increment; (B) NLHR

evident in the examination of the 450 and 550 mb thermal advection fields (not shown). Examining the 450 and 550 mb levels is sufficient, since DTAD is calculated in this study over a 100 mb layer, not the entire lower troposphere. At 550 to 450 mb the temperature field is nearly in phase with the height field, resulting in weak advection. WAA increasing with height may be a result of increasing wind speed with height. Additionally, propagation effects supplement height falls. The height tendency difference field for DTAD (Fig. 20 C, thin lines) shows a small region of negative difference, owing to slightly larger height falls in the OPNL run near the trough, and canceling out propagation effects.

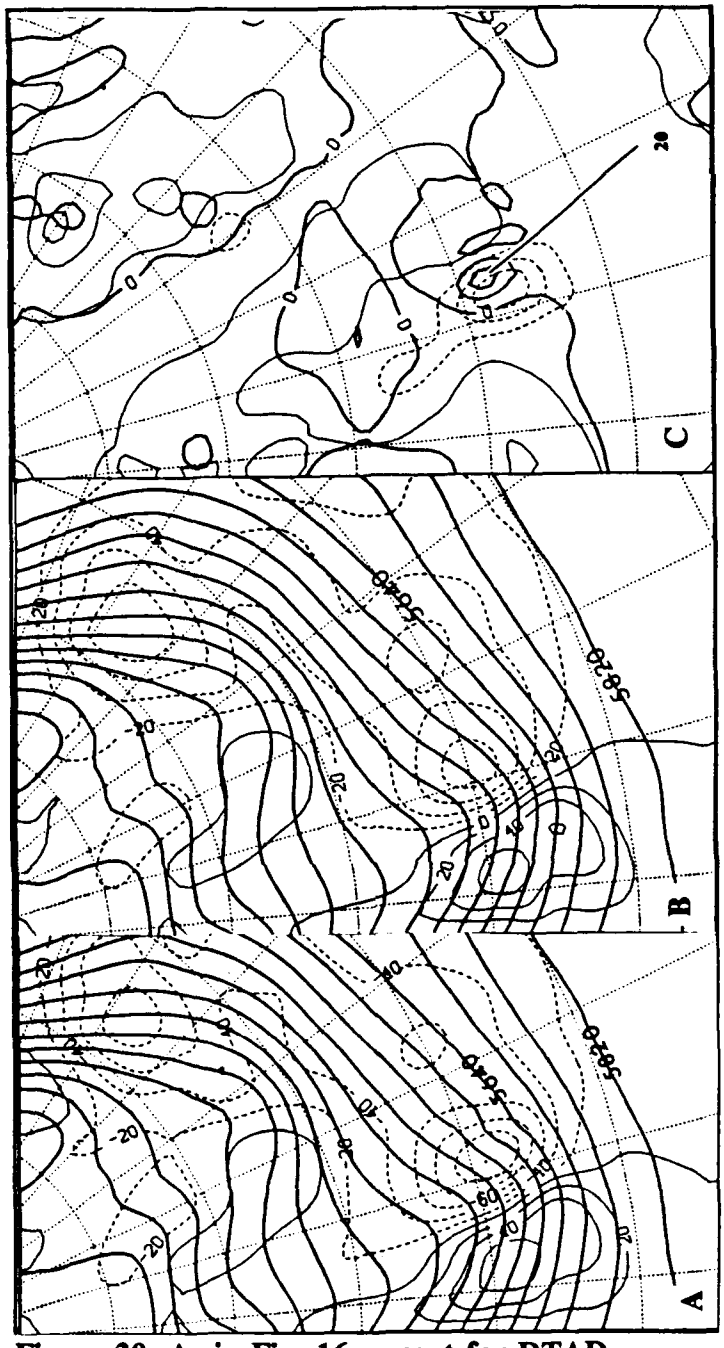

Figure 20. As in Fig. 16, except for DTAD

The contribution to the height tendency by the next term, (ω dσ/dp) (DSIG) (Fig. 22 A,B) is related to adiabatic heating and cooling effects, and in general acts to limit

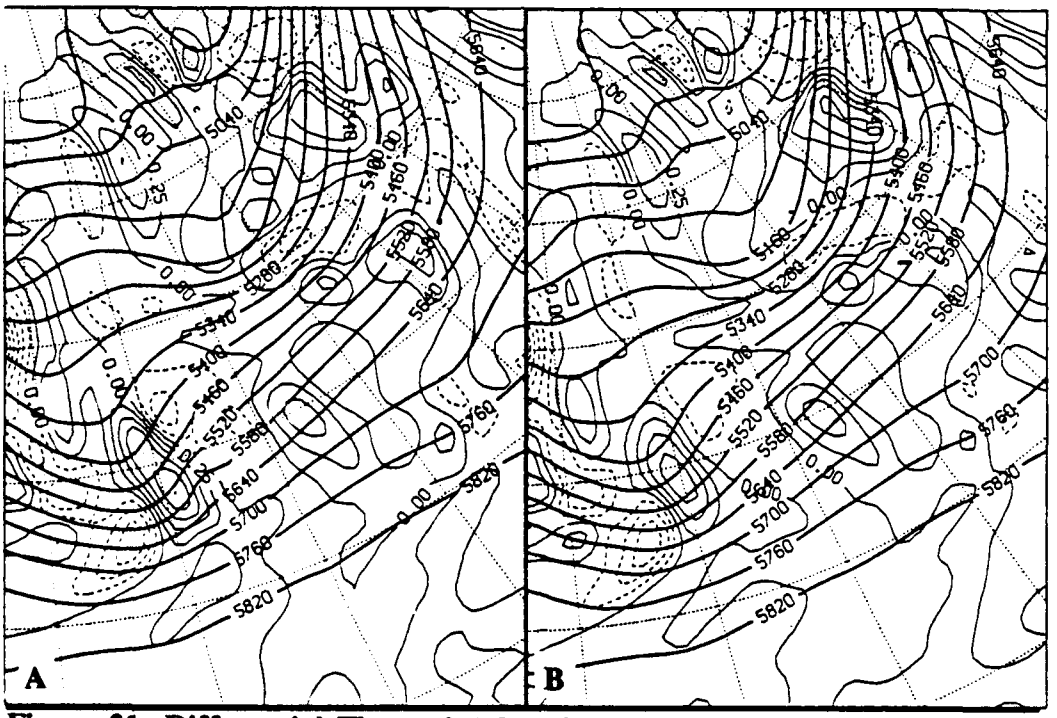

Figure 21. Differential Thermal Advection at 500 mb, 24 h forecast: (A) OPNL, heights (bold), 6 dm increment, and differential thermal advection (thin, dashed negative), 0.25×10^{-12} s^{-3} increment; (B) NLHR

the height tendencies. If σ increases with height, as it usually does, the sign of this term is determined by the sign of the vertical motion, yielding height rises in regions of upward motion, and height falls in regions of downward motion. Not surprisingly, the DSIG field in this case has its maximum downstream of the trough and its minimum upstream of the trough, opposite to the previous two terms. The amplitude and location of DSIG features serve to almost entirely offset the height tendencies resulting from the DTAD field. The stronger upward motion present in the OPNL case yields stronger height rises downstream of the trough, as can be seen from the difference fields (Fig. 22 C).

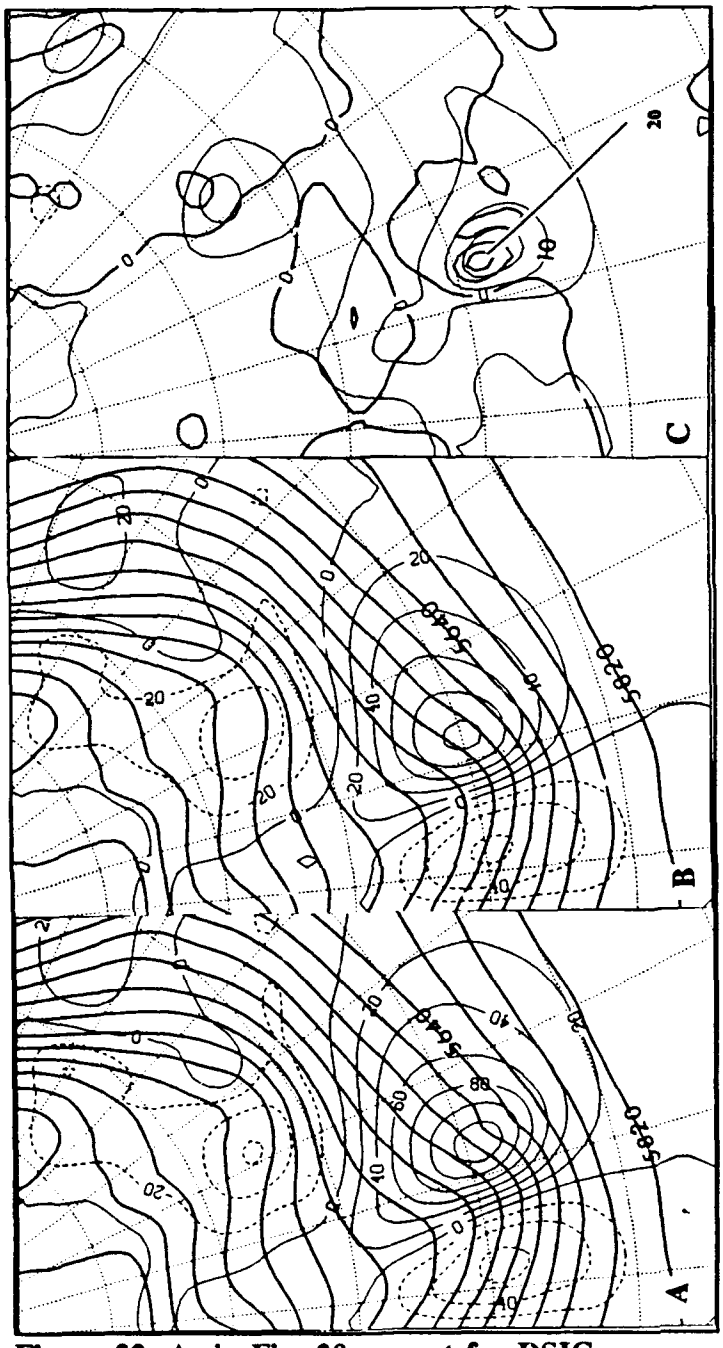

Figure 22. As in Fig. 20, except for DSIG

The final terms considered are the diabatic heating (DQTOT), vertical advection of vorticity (DZET), and the tilting term (TILT). These terms are one-third to one-fifth

of the magnitude of the other terms, with smaller differences between the OPNL and NLHR runs, and so are not shown. DQTOT provides a maximum of +15 m/12 h height tendency, a very small direct affect of LHR. Not surprisingly, the DQTOT height tendency maximum is centered on the positive height anomaly, and elongated parallel to and just downstream of the trough axis. Height rises from DQTOT indicate that the heating maximum occurs at a level below 500 mb. DZET and TILT height tendencies are small, less than 20 m/12 h over the region in both OPNL and NLHR runs, and difference fields between the two runs (not shown) indicate that the effect of LHR on these two terms tends to oppose; the major feature of TILT is a +10 m /12 h difference, while the major feature of the DZET is a -10 m /12 h difference in nearly the same area.

In summary, the major contributor to the total height tendency for the 24 h forecast is that due to ZADV, with height falls ahead of the trough and height rises behind. The magnitude and pattern of DTAD height tendencies was similar to the ZADV fields, but the effect of DTAD is almost totally offset by DSIG. DSIG height tendencies are of nearly the same magnitude as DTAD, but of opposite sign. DQTOT, DZET, and TILT were found to be much smaller than the previous three terms, with the latter two tending to offset each other. DQTOT provided small height rise tendencies downstream of the trough in the region of the height anomaly.

B. 36 h FORECAST

The total height tendency pattern for the 36 h forecast (Fig. 23 A,B) is more symmetric about the trough than it was in the 24 h forecast. The OPNL run shows

height falls in and just downstream of the 500 mb trough, suggesting further trough intensification; the NLHR height tendencies are nearly zero at the trough line, and much weaker than the OPNL run downstream of the trough. Additionally, although the height rise/fall pattern appears nearly symmetric in the OPNL run, height falls along a given contour are greater than height rises in the northern part of the trough. This is especially evident near the height anomaly, the sharp bend in the 5400 m contour. As in the 24 h forecast, a height anomaly is coincident with a local maximum in the precipitation forecast field, confirming its relationship to LHR; the height anomaly is situated near a 28.45 mm/12 h (1.12 in/ 12 h) precipitation maximum. As in the 24 h forecast, maximum height falls are substantially greater in the OPNL run than in the NLHR run; the OPNL version of the storm should continue to intensify at a greater rate than the NLHR version. In fact, the height falls in the NLHR version are weaker than height rises upstream of the trough, suggesting a potential weakening of the trough.

The values in the OPNL-NLHR difference field (Fig. 23 C) are much larger than for the 24 h forecast. The 500 mb height difference shows a -30 m difference in the base of the trough, and a +20 m difference in the downstream ridge, reflecting the increased amplitude in both trough and ridge in the OPNL forecast. Again, height differences occur primarily downstream of the trough. The OPNL run (Fig. 23 A) shows large negative height tendencies in the area of the height anomaly, while the NLHR run (Fig. 23 B) has one local negative maximum in nearly the same area, but a larger second maximum much farther away from the trough. Thus, the height tendency difference field (Fig. 23 C) resembles the OPNL height tendencies in this area. Farther

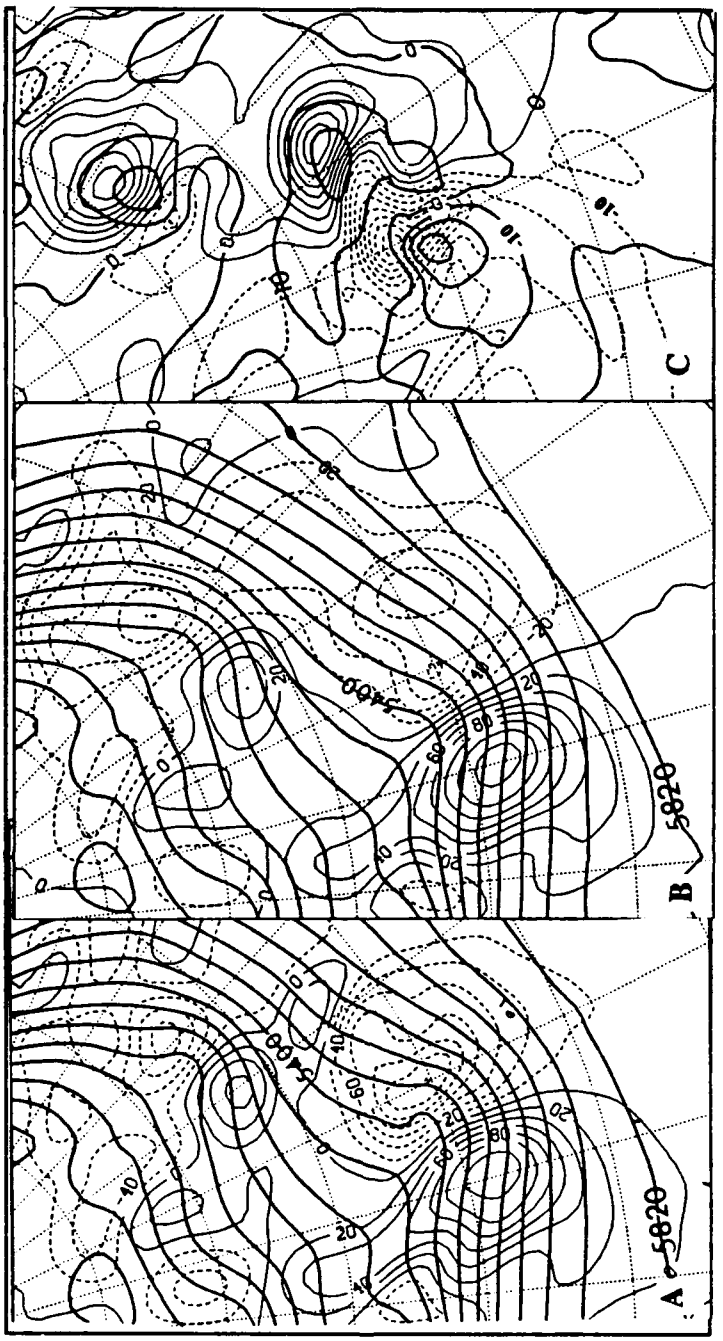

Figure 23. As in Fig. 22, except Total Height Tendency Fields, 36 h forecast

downstream of the trough past the ridge axis, positive height tendency differences occur as a result of significant ridging in the OPNL run. Negative height tendency differences upstream of the trough derive from the NLHR run's stronger height rises.

The 12 h height change field (Fig. 15 C) for the OPNL run shows greater height falls than rises, whereas the instantaneous OPNL (Fig. 23 A) run showed more symmetry about the trough. This disparity between the time averaged 12 h height difference field and the instantaneous height tendency pattern demonstrates the effect of varying intensification rate on the two methods. The NLHR 12 h height change field (Fig. 15 D) shows height rises exceeding height falls, indicating decreasing intensity. The instantaneous height tendency pattern (Fig. 23 B) shows even greater height rises than falls. Clearly the OPNL and NLHR runs are diverging; the OPNL run shows signs of strong intensification of the 500 mb trough, while the NLHR run already shows evidence of weakening.

The forcing terms play much the same roles in the 36 h forecast as they did in the 24 h forecast. Vorticity advection (ZADV) again accounts for most of the total height tendency. Both OPNL (Fig. 24 A) and NLHR (Fig. 24 B) runs show height falls in the PVA region, as expected, but the OPNL run develops height falls one-third larger than the NLHR run. The OPNL-NLHR difference field (Fig. 24 C) again shows negative differences reflecting the much larger height falls in the OPNL field in and just downstream of the 500 mb trough. Positive differences are found downstream of the downstream ridge axis in the OPNL run, reflecting the weak height falls in the NLHR run and significant height rises in the OPNL run.

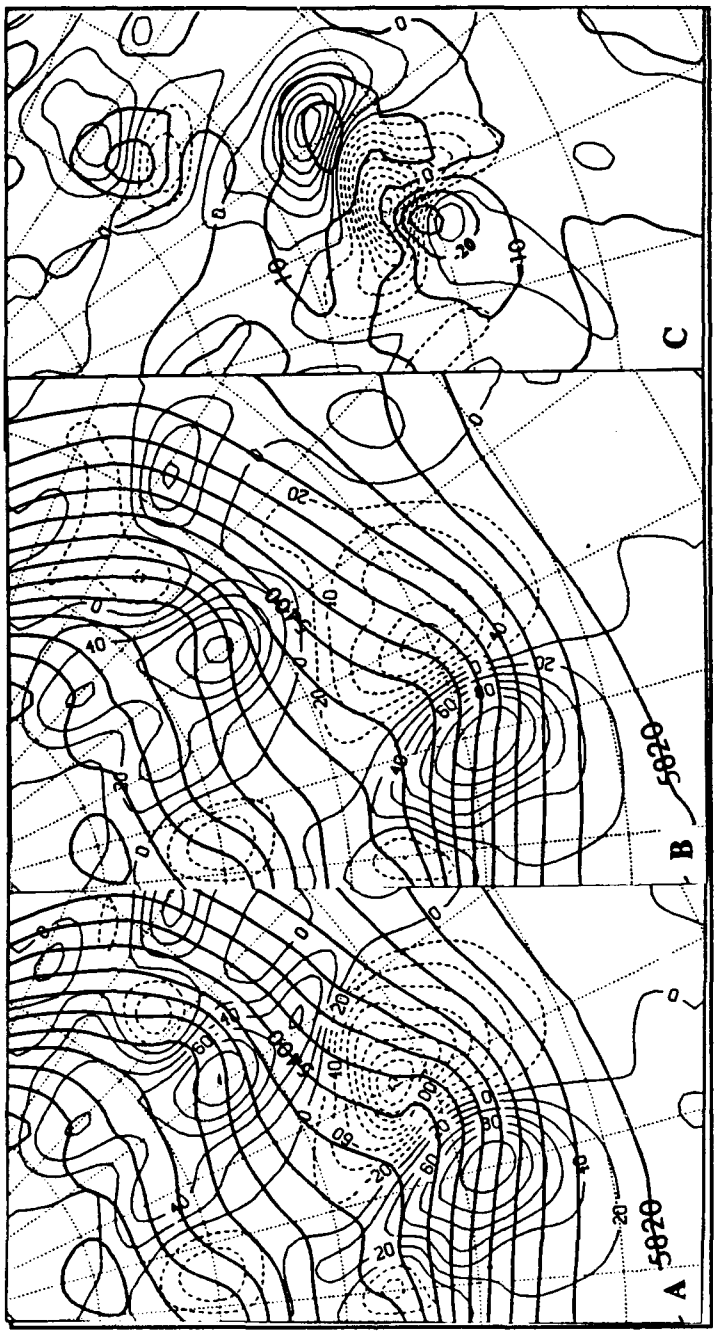

Figure 24. As in Fig. 23, except for ZADV

The OPNL ZADV height fall maximum is again located near the height anomaly; the 500 mb relative vorticity field depicts a strong vorticity gradient centered on the

height anomaly, and much stronger PVA in the OPNL run (Fig. 25 A) than in the NLHR run (Fig. 25 B). Importantly, the height rise patterns upstream of the trough are nearly identical in both runs; no LHR effects were expected there.

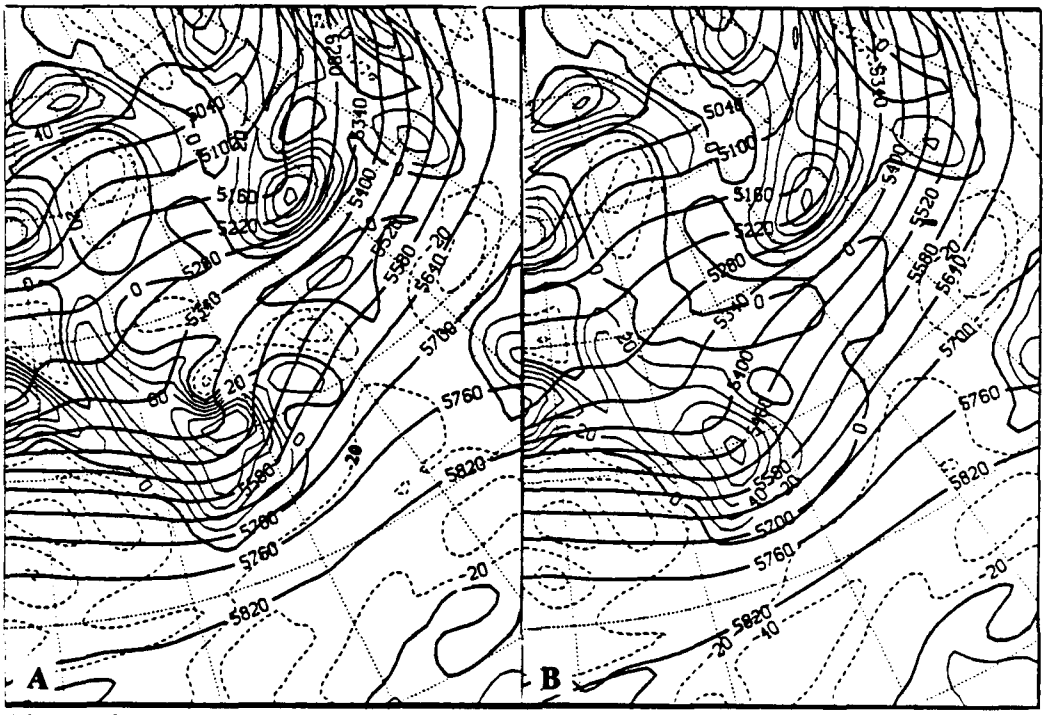

Figure 25. As in Fig. 18, except 36 h forecast

The differential thermal advection (DTAD) height tendencies (Fig. 26 A,B) are only half the magnitude of the ZADV height tendencies at this forecast time, reconfirming vorticity's dominant role. The DTAD fields are of roughly the same magnitudes upstream of the trough for the OPNL and NLHR runs. Downstream, however, the OPNL run shows height falls one-third larger than in the NLHR run. Further, the intensity of the height falls was greater than that of the 24 h forecast. The same processes are at work in the 36 h forecast as in the 24 h forecast; continued forcing differences between the OPNL and NLHR runs over time cause the solutions to diverge.

The height anomaly associated with LHR grew in the 12 h between forecasts, increasing WAA downstream of the trough. The DTAD OPNL height fall gradient is much stronger than the NLHR gradient, and the OPNL height fall maximum is much closer to the trough than in the NLHR run. Consequently, the OPNL-NLHR difference (Fig. 26 C) field reveals much larger differences than in the 24 h forecast. The region of negative height tendency difference (OPNL height falls greater than NLHR height falls) extends along and downstream of the trough, covering a much larger area than in the 24 h forecast. As in ZADV, positive differences occur downstream of the ridge axis, due to the moderate height falls present over a broad region in the NLHR run being subtracted from the smaller height falls in the OPNL run's more intense but narrower ridge.

The DSIG height tendency fields (Fig. 27 A,B) have the expected opposite polarity resulting from upward motion downstream of the trough, opposing previous terms. Due to the differences in upward motion between the OPNL and NLHR runs, the magnitude of the forcing downstream of the trough is much greater in the OPNL run (Fig. 27 A) than in the NLHR run (Fig. 27 B). The amplitude and location of features in the DSIG field again serve to almost entirely offset the height tendencies associated with DTAD, even though both DSIG and DTAD fields are of moderate magnitude. The DSIG difference field (Fig. 27 C) reflects the much greater forcing by the OPNL run downstream of the 500 mb trough. Diabatic heating (DQTOT) (not shown) is once again found in the region of the height anomaly, contributing about +20 m / 12 h to height tendency. Again, this direct effect of LHR is very small compared to the indirect effects. DZET and TILT are also quite small in comparison to the other terms and

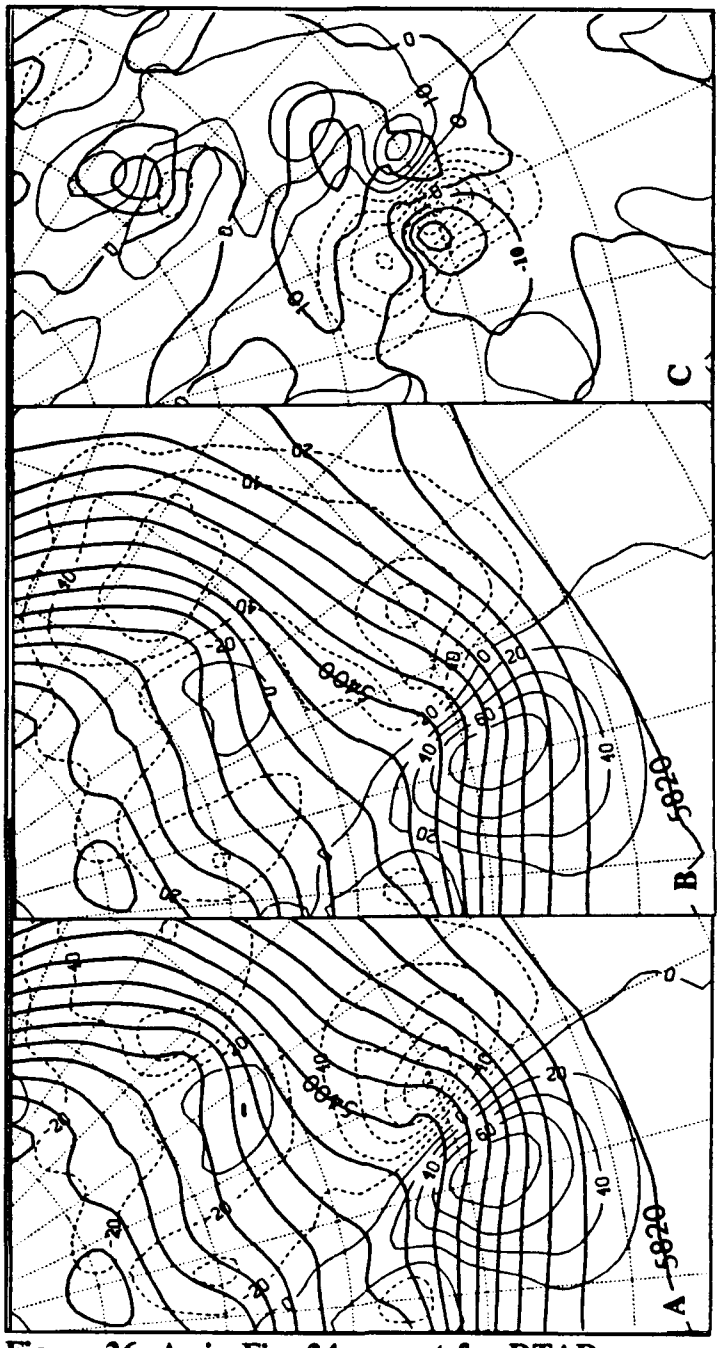

Figure 26. As in Fig. 24, except for DTAD

nearly negligible in the NLHR run; the terms have opposite magnitudes and cancel each other, leaving vorticity advection as the single greatest influence on the total height tendency, modified somewhat by the sum of DTAD and DSIG.

As in the 24 h forecast, ZADV was the greatest influence on the total height tendency, followed by DTAD, which was offset by DSIG. DQTOT, DZET, and TILT again were small in comparison to the other terms. DQTOT again contributed modest height rise tendencies downstream of the trough in the area of the height anomaly.

C. 48 h FORECAST

By the 48 h forecast, the time of maximum intensity of the observed surface cyclone, the OPNL run's 500 mb wave had propagated east, rotated its axis to NW/SE, amplified its downstream ridge, and produced a closed low (Fig. 28 A, thick lines). During the same period, however, the NLHR wave (Fig. 28 B, thick lines) had propagated east and weakened. Comparison with the 12 h height change pattern cannot be accomplished for the 48 h forecast time; the 6 h bracketing of synoptic times used to generate the height change field is impossible since the forecast extends only to 48 h. The OPNL height tendency pattern (Fig. 28 A) is fairly symmetric, suggesting some slight further development. An important feature is the closed low; however, it is not the focus of forcing since the cyclone is almost vertically stacked. The height fall maximum is not immediately downstream of the closed low, but downstream of the center of the trough. In the OPNL run height falls remain slightly greater than rises along a given contour, reflecting in part the asymmetry between the upstream and downstream ridges. As in the

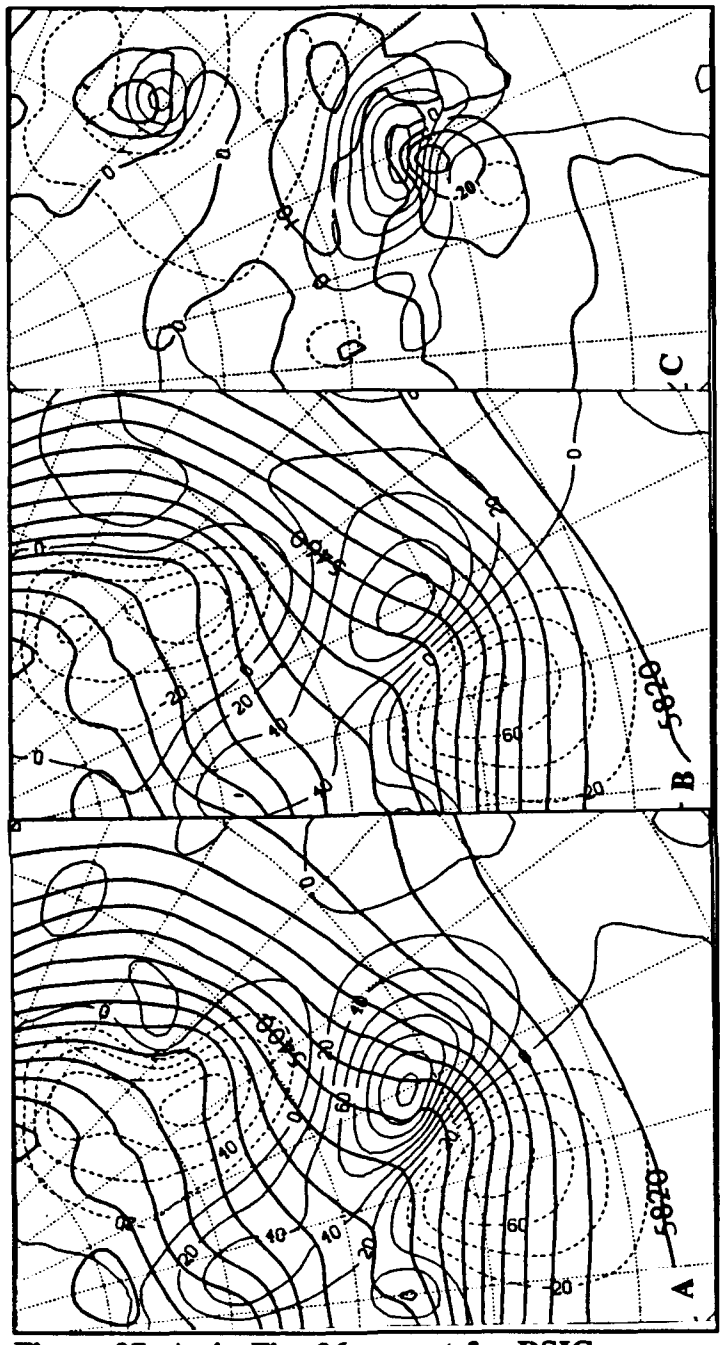

Figure 27. As in Fig. 26, except for DSIG

24 h and 36 h forecasts, height falls are greater in the OPNL run than the NLHR run; the NLHR run's height falls (Fig. 28 B) are only half those of the OPNL run's and are

centered farther downstream. Further, in the NLHR run height rises are twice as large as height falls, and intrude into the trough, suggesting cyclolysis.

The OPNL-NLHR difference field (Fig. 28 C) shows much larger differences than either the 24 h or 36 h forecasts. The 500 mb height difference shows a -90 m difference in the trough, and a +30 m difference in the downstream ridge; the NLHR run failed to develop a significant upper-level wave and even weakened the amplitude of the pre-existing wave. Negative height tendency differences are found just downstream of the closed low, reflecting the OPNL run's much greater height falls. Positive height tendency differences are located far downstream of the ridge axis, owing to a combination of steep ridging and the proximity of a trough downstream. An area of negative height tendency is found upstream of the trough, a result of the NLHR run's greater height rises. Since the OPNL and NLHR runs' height rises are of nearly the same magnitude upstream of the trough, the sign of the difference field changes frequently, resulting in positive height tendency differences sandwiched between two groups of negative contours.

Vorticity advection (ZADV) (Fig. 29 A,B) again accounts for most of the total height tendency. Both OPNL and NLHR runs show height falls in the PVA region, as expected, but the OPNL run (Fig. 29 A) develops height falls one-third larger than the NLHR run (Fig. 29 B). In the OPNL run, the height fall maximum associated with ZADV is located just downstream of the trough. As before, the height rise patterns upstream of the trough are quite similar in both runs; no LHR effects were expected there. The OPNL-NLHR difference field (Fig. 29 C) again shows large negative

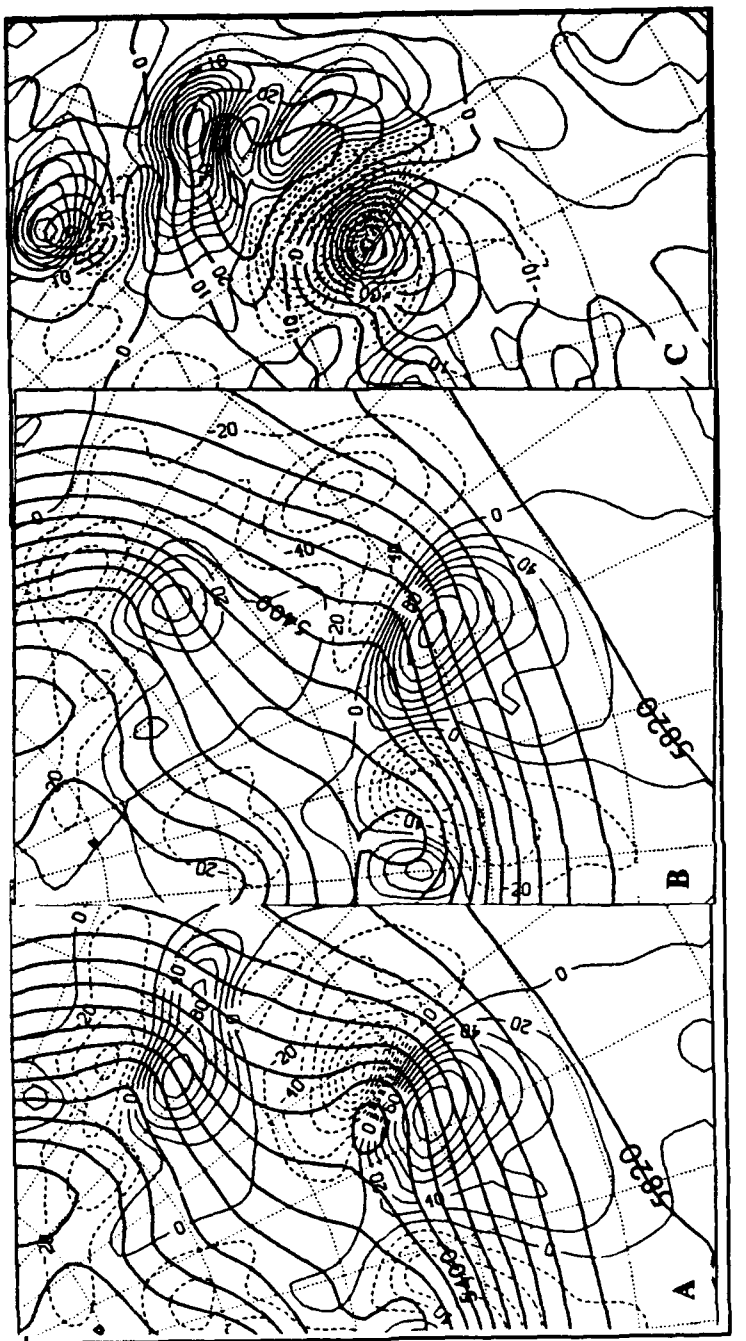

Figure 28. As in Fig. 27, except for Total Height Tendency Fields, 48 h Forecast

differences downstream of the 500 mb trough and large positive differences downstream of the ridge, reflecting the stronger height tendencies in the OPNL run. The negative

values in the difference field extend west of the trough, since both the OPNL and NLHR runs connect PVA from the downstream trough to the upstream trough, the OPNL run's PVA being more intense. Additionally, phase differences in the height tendency fields (NLHR lagging downstream of the trough but leading upstream of the trough) also are sources of negative values.

The differences in the OPNL and NLHR runs may be explained by examining the forcing fields. The vorticity fields reveal a vorticity maximum at the base of the closed low in the OPNL run (Fig. 30 A), extending well west and merging with the maximum at the base of the upstream trough. Negative vorticity is prominent in the downstream ridge, extending westward north of the closed low. In the NLHR run (Fig. 30 B), positive vorticity is much weaker in the trough of interest, but greater in the upstream trough near the western boundary of the domain. (The fact that the NLHR run's development of this closed feature is greater than the OPNL run is surprising. Since this feature entered the computational domain at the 48 h forecast time, little data are available in this study to determine its origin.) The NLHR run has only slight negative vorticity in its weak ridge. The vorticity advection fields show much stronger PVA downstream of the trough in the OPNL run (Fig. 31 A), as expected, but this PVA also extends north of the closed low. The NLHR run (Fig.31 B), with weaker vorticity and vorticity gradients, also has weaker vorticity advection.

The DTAD height tendencies (Fig. 32 A,B) are of roughly the same magnitudes upstream of the trough for the OPNL and NLHR runs, and are comparable to fields from previous forecast times. The OPNL DTAD field (Fig. 32 A) is quite symmetric about

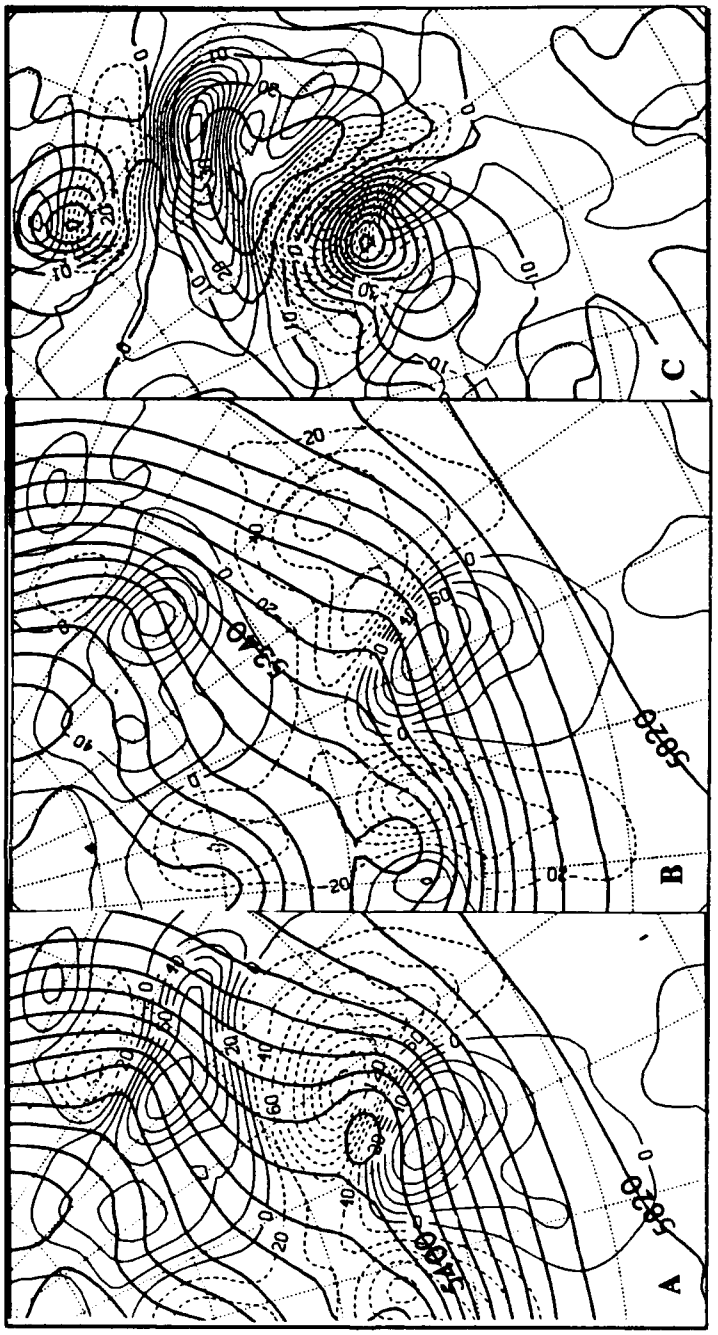

Figure 29. As in Fig. 28, except for ZADV

the trough, while the NLHR field (Fig. 32 B) has a weaker maximum located much farther downstream of the trough. The DTAD difference fields (Fig. 32 C) show large

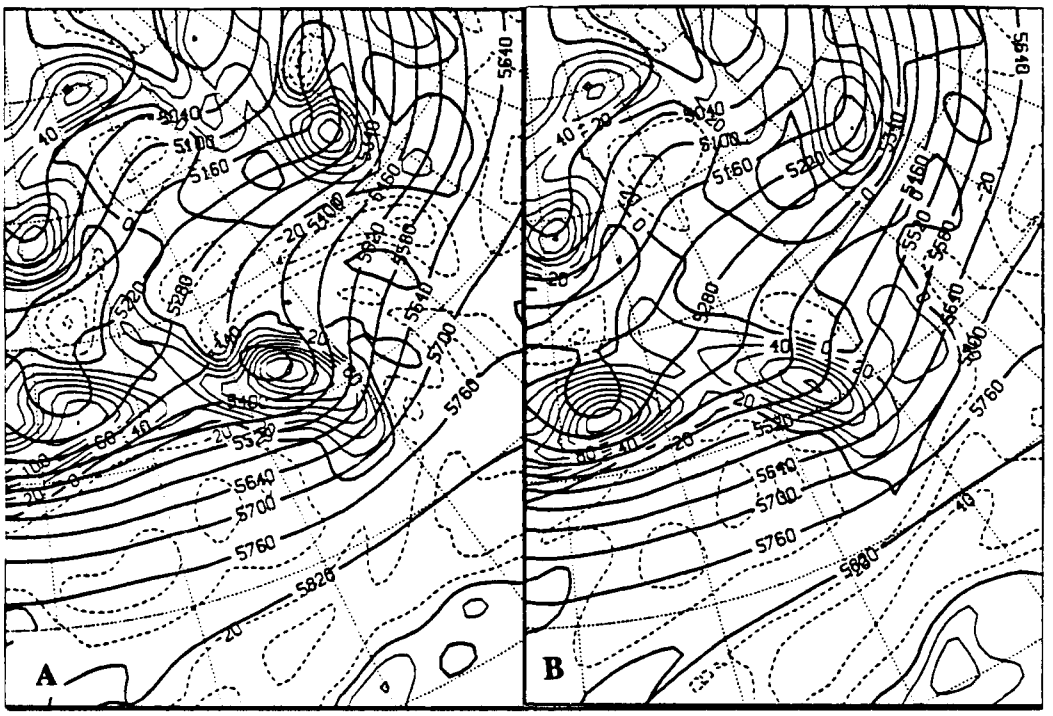

Figure 30. As in Fig. 25, except 48 h forecast

negative values downstream of the rough, stemming from the weakness of the NLHR field compared to the large height falls of the OPNL field. Farther downstream, small positive values result since the OPNL run's greater height falls are concentrated closer to the trough, while the less intense height falls in the NLHR run taper off more gradually. Upstream of the trough, positive and negative height fall differences alternate, a result of phase differences between OPNL and NLHR height rises.

The temperature advection fields at 500 mb (not shown) for the OPNL and NLHR runs reveal that the magnitudes of WAA near the trough are similar in each run, but the WAA maximum is located at the ridge axis in the OPNL run, aiding ridge building, while the WAA maximum is found in the trough in the NLHR run, indicating cyclolysis. As in the 24 h and 36 h forecasts, differential thermal advection fields (not shown) depict

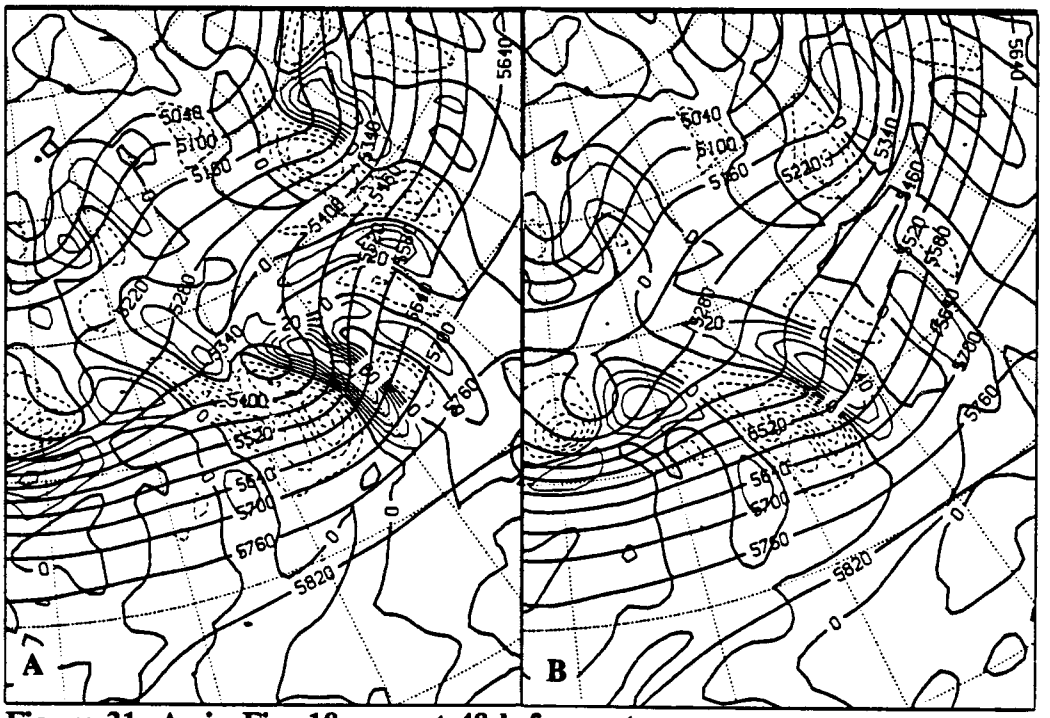

Figure 31. As in Fig. 18, except 48 h forecast

positive forcing downstream of the trough, leading to height falls.

The DSIG field (Fig. 33 A,B) is very asymmetric, with height rises three times larger than height falls in the OPNL run (Fig. 33 A), and height rises two times larger than falls in the NLHR run (Fig. 33 B). The vertical motions combined with a weakening of the vertical gradient of static stability may account for the disparity, especially in the OPNL run. The DSIG difference field (Fig. 33 C) shows the large difference in downstream forcing between the OPNL and NLHR runs, resulting in a +70 m/12 h difference. Upstream of the trough, small negative values occur, owing to the OPNL run's slightly greater height falls. Evidence of weaker vertical motion is also found in the weaker DQTOT, DZET, and TILT fields (Fig. 34 A,B,C). DQTOT supplied a maximum of +15 m /12 h to height rises in the ridge, a decrease over the

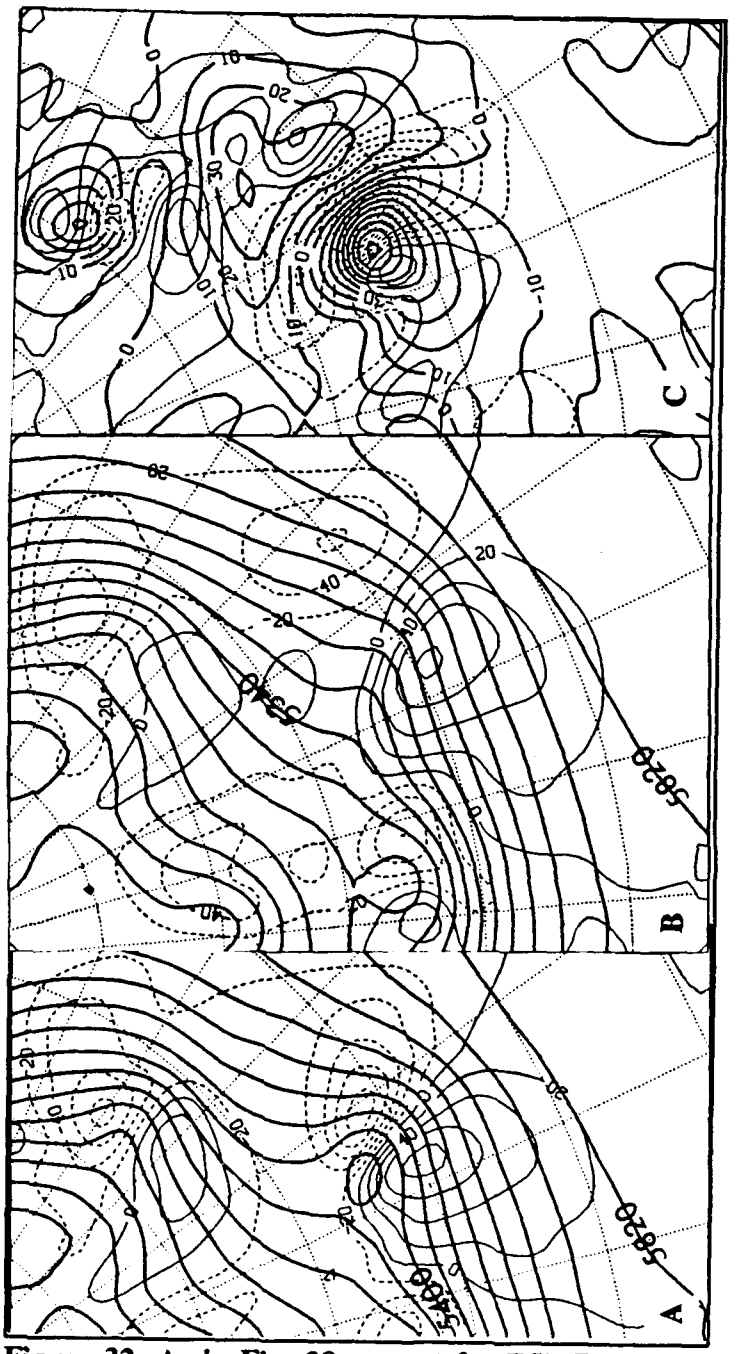

Figure 32. As in Fig. 29, except for DTAD

previous 12 h which again shows the limited direct effects of LHR. As before, the DZET and TILT fields are small, and tend to cancel each other out.

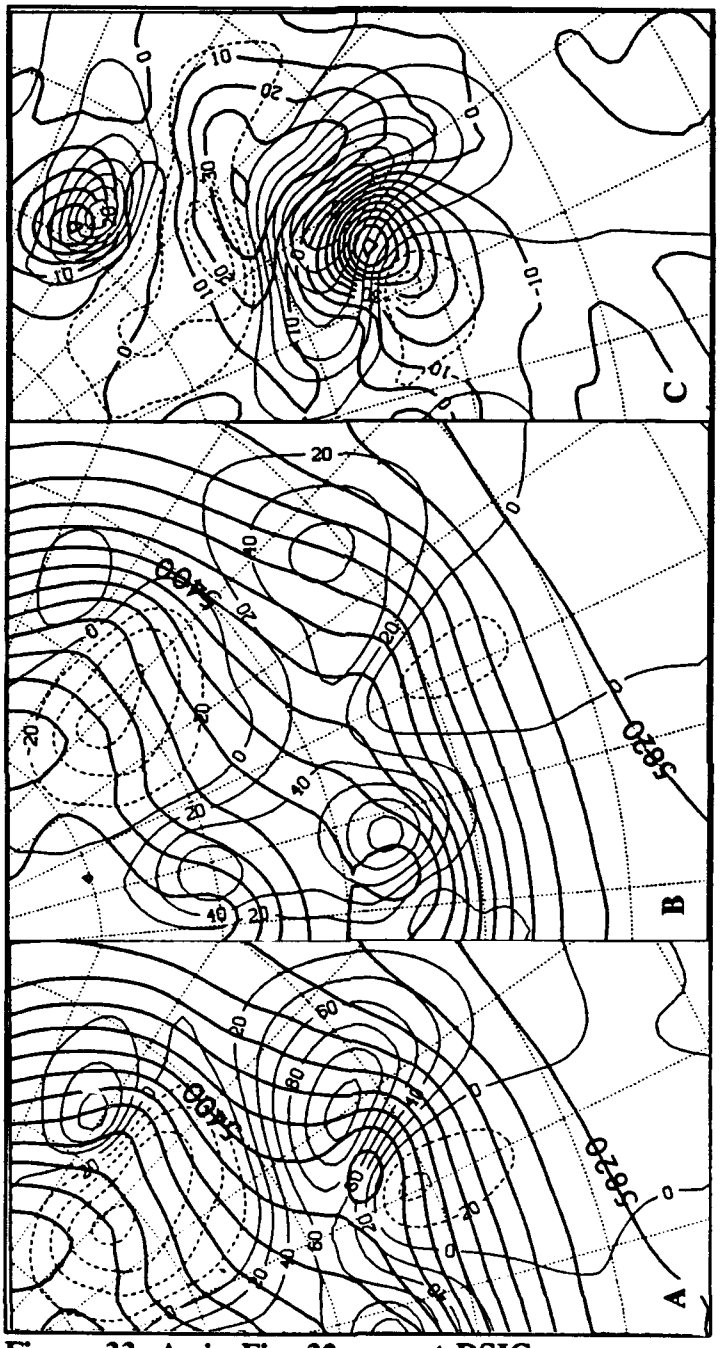

Figure 33. As in Fig. 32, except DSIG

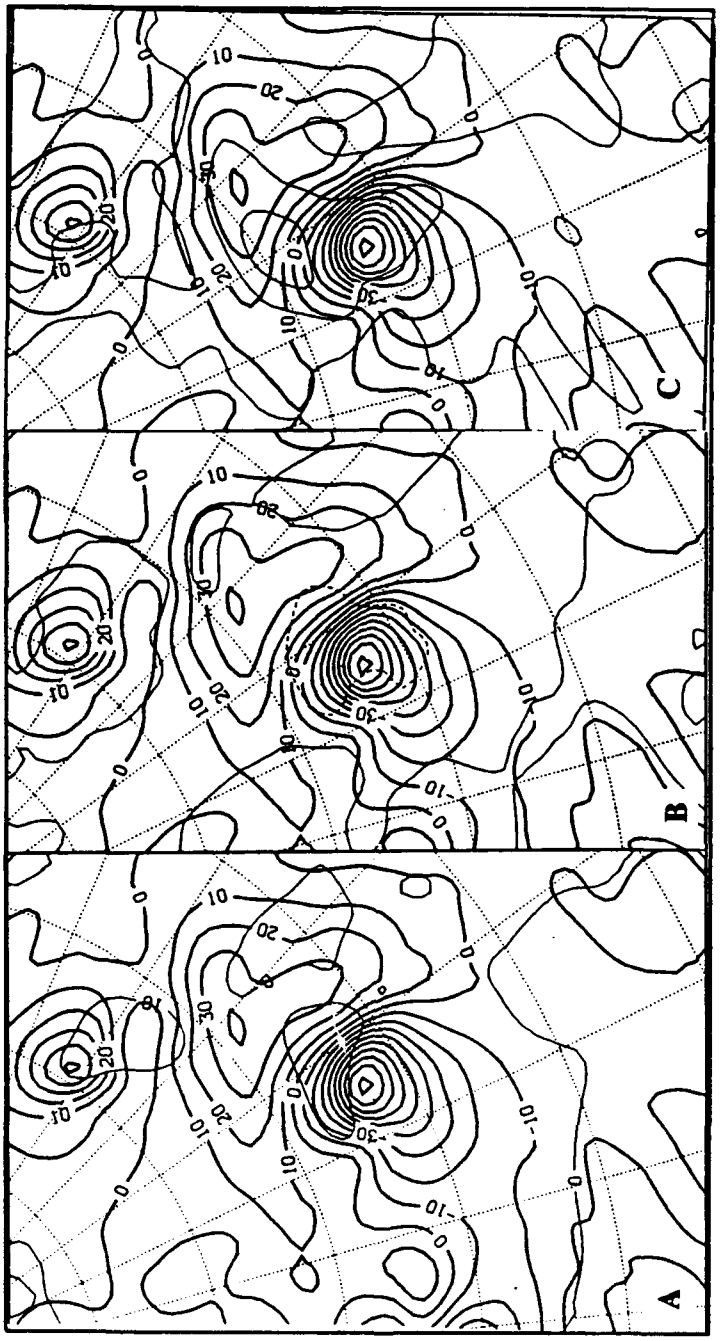

Figure 34. DQTOT, DZET, and TILT Height and Height Tendency Difference Fields at 500 mb: (A) DQTOT height differences (bold) 1 dm increment, and height tendency differences (thin, dashed negative) 10 m/12 h increment; (B) DZET; (C) TILT

The roles of the various terms in the height tendency equation remained consistent over the 48 h period, with ZADV affecting total height falls the most, with DTAD and

DSIG nearly offsetting each other. DQTOT, DZET, and TILT were all much smaller than the three previous terms, with DZET and TILT partly offsetting each other. DQTOT consistently provided small height rise tendencies over the 48 h, peaking at 36 h. The focus of DQTOT height rises was the height anomalies in the 24 and 36 h forecasts, and downstream of the trough in the 48 h forecast.

VI. CONCLUSIONS

A. DISCUSSION AND CONCLUSIONS

This study examined the height tendencies in a rapidly intensifying oceanic cyclone whose central pressure dropped 35 mb in 48 h. Over the 48 h, latent heat release accounted for a height fall of over 90 m in the 500 mb trough and a height rise of 40 m in the ridge. These results are in agreement with Chang et al. (1982) and Robertson and Smith (1983), who found latent heat release increased the amplitude of the 500 mb wave by deepening the trough as well as raising the ridge, although not quite to the extent of this case.

The analysis of height tendencies by the generalized height tendency equation showed that vorticity advection was the primary forcing term responsible for the height rises and falls at all three synoptic times. Differential thermal advection had significant magnitude at most synoptic times, but was almost completely offset by the vertical advection of static stability, which acted to limit intensification and propagation. The direct role of differential heating through the diabatic term was a small one at 500 mb, contributing slight height rises just downstream of the trough. The contributions of the vertical advection of vorticity and the tilting term were negligible. These findings concur with Pauley and Smith (1988) and Tsou et al.(1987).

The hierarchy of importance of the various terms remained the same for both the operational (OPNL) and no latent heating model (NLHR) runs, yet the magnitude of the

height tendencies associated with individual forcing terms was quite different between the two runs. Importantly, early in the forecast most of the maxima in height tendency terms in the OPNL run were situated at or near a small-scale bend in a height line just downstream of the trough. At the 24 h forecast, the height anomaly consisted of a small-scale bend in the 5580 m contour; most of the differences between the OPNL and NLHR fields are small and in the area of the height anomaly. At the 36 h forecast, a much larger, but still small-scale bend was found in the 5400 m contour. Significant height tendency differences were found in the vicinity of this feature. By the 48 h forecast, the two fields had developed so differently in response to different forcing that the concept of height anomaly had no meaning.

The height anomalies presumably owe their origin to latent heat release, since they were present in OPNL but not NLHR runs. Latent heat release lower in the atmosphere tends to increase geopotential heights above the level of maximum LHR and decrease height below. While LHR tends to inflate the entire ridge, the height anomalies may have been "hot spots" of particularly intense forcing. These "hot spots" coincided with local maxima in the precipitation forecast in the 24 and 36 h forecasts.

The fact that some extratropical cyclones are quite sensitive to latent heating while others are not is an impediment to more accurate forecasting. Certainly the amount and vertical location of LHR are important in determining development, as many studies have shown. Perhaps equally important is the horizontal location of the LHR, relative to the trough and the mean flow.

In the IOP-5 cyclone, LHR caused height anomalies at 500 mb with concomitant anticyclonic vorticity. Since the anomaly was just downstream of the 500 mb trough, the anticyclonic vorticity maximum was directly downstream of the cyclonic vorticity maximum in the trough, tightening the vorticity gradient, and thereby increasing positive vorticity advection and height falls.

A different geometry is present in the storm studied by Pauley and Smith (1988). In that storm, the LHR is farther downstream from the trough, and not directly downstream of the vorticity maximum. The anticyclonic vorticity in the region of LHR increases the vorticity gradient more parallel to the mean flow, resulting in limited advection differences. Among the authors' conclusions was that the storm was not particularly sensitive to diabatic effects. A particular cyclone's sensitivity to LHR may well depend on this interplay between the geographic location of the LHR and the location of the short-wave vorticity maximum aloft.

B. RECOMMENDATIONS

1. This study focused on the effect of LHR on the 500 mb wave. Tsou et al. found that the roles of the various height tendency equation terms were the same throughout the troposphere; further study of this case should be directed at examining LHR effects at other levels, particularly in the lower atmosphere, closer to the level of maximum LHR.

2. Although the OPNL forecast was a great improvement over the NLHR forecast, the OPNL forecast still did a poor job of predicting the location and intensity of the IOP-5 storm. A comparison of the 48 h forecast and NGM analyses valid at 12Z/20 shows that the upper-level trough and downstream ridge were both underpredicted, suggesting a deficiency in the forecast related to LHR. Experiments should be conducted with the NGM or a similar model to assess the

effects of increasing the amount of LHR, and varying the horizontal and vertical locations, in an attempt to produce a forecast which shows more fidelity to the observed storm.

3. To test the hypothesis that the horizontal location is important to intensification, other rapidly deepening cyclones should be examined for sensitivity to the 500 mb trough/mean flow/LHR geometry. Constructing composite storms to identify the typical geometry of rapidly deepening storms versus non-rapidly deepening storms would be useful for accomplishing this task.

APPENDIX: THE NESTED GRID MODEL (NGM)

The salient aspects of the NGM as described by Hoke et al. (1989) are:

- 48 h forecast
- 3 nested grids: A-grid covering the northern hemisphere, 336 km resolution at 45°N
  B-grid double resolution of A-grid
  C-grid double resolution of B-grid, 84 km gridpoint spacing at 45°N
- 16 layers, 13 in troposphere, varying layer thickness with greatest resolution at the bottom of the atmosphere
- Fixed depth planetary boundary layer (4 layers)
- Differencing: Arakawa D-grid with Lax-Wendroff time differencing
- Inner grid time-step: 75 sec
- 6 h forecast first guess
- Objective analysis: Regional Optimal Interpolation
- Normal mode initialization
- Stability dependent fluxes, bulk surface exchange
- Kuo (1965) cumulus parameterization, large scale precipitation, dry convective adjustment

The Kuo cumulus parameterization scheme merits further discussion, being so pertinent to the issue of LHR. Hoke et al. (1989) presented the following description of their implementation of the Kuo scheme: "Moist convection occurs at a model grid point when 1) there is sufficient convergence of moisture in the bottom six layers of the model;

2) a parcel originating in any of the lowest four layers of the model would become buoyant if lifted (convective instability), and 3) total moisture convergence into the column below the cloud top is positive."

Moisture is redistributed in the vertical in the form of LHR and moistening. 80% of moisture is converted to precipitation with accompanying LHR. This 80% is distributed vertically, proportional to the difference between cloud temperature and model temperature in each layer for the warmest adiabat from the lowest four layers. 20% of the moistening is distributed vertically according to the difference between specific humidity of the cloud and the model (Hoke et al. 1989).

Convective precipitation falls and evaporates into lower layers until the relative humidity reaches 48%, then proceeds to next lower layer. Grid-scale precipitation occurs when the relative humidity at a grid point exceeds 95%. Supersaturation is not allowed. The precipitation falls and evaporates in to the next lower layer until the relative humidity there reaches 95%. Clouds are inferred when relative humidity is greater that 80% (Hoke et al. 1989).

REFERENCES

Anthes, R.A., Kuo, Y-.H., and Benjamin, S.G., 1982: Explosive cyclogenesis over the west-central North Atlantic Ocean, 1981-1984. Part II: Evaluation of LFM model performance. *Mon. Wea. Rev.*, **110**, 1187-1213.

Anthes, R.A., Kuo, Y-.H., and Gyakum, J.R., 1983: Numerical simulations of a case of explosive marine cyclogenesis. *Mon. Wea. Rev.*, **111**, 1174-1188.

Auciello, E.P., 1991: A forecast checklist for predicting meteorological bombs in the western North Atlantic. Preprints of the First International Winter Storm Symposium, New Orleans, Amer. Meteor. Soc., 306-308.

Chang, C.B., Perkey, D.J., and Kreitzberg, C.W., 1982: A numerical case study of the effects of latent heating on a developing wave cyclone. *J. Atmos. Sci.*, **39**, 1555-1570.

_____, 1984: Latent heat induced energy transformations during cyclogenesis. *Mon. Wea. Rev.*, **112**, 357-367.

Chen, T-.S., Chang, C.B., and Perkey, D.J., 1983: Numerical study of an AMTEX '75 oceanic cyclone. *Mon. Wea. Rev.*, **111**, 1818-1829.

Dare, P.M., and Smith, P.J., 1984: A comparison of observed and model energy balance for an extratropical cyclone system. *Mon. Wea. Rev.*, **112**, 1289-1308.

Grell, G, Reed, R.J., and Kuo, Y-.H., 1991: Numerical experiments on the ERICA IOP-5 storm: a surprise rapid deepener. Preprints of the First International Winter Storm Symposium, New Orleans, Amer. Meteor. Soc., 414-417.

Gyakum, J.R., 1983: On the evaluation of the QE II storm. I: synoptic aspects. *Mon. Wea. Rev.*, **111**, 1137-1155.

Hadlock, R., and Kreitzberg, C.W., 1988: The experiment on rapidly intensifying cyclones over the Atlantic (ERICA) field study: objectives and plans. *Bull. Amer. Meteor. Soc.*, **69**, 1309-1320.

Hoke, J.E., N.A. Phillips, G.J. DiMego, J.J. Tuccillo, and J.G. Sela, 1989: The regional analysis and forecast system of the National Meteorological Center. *Weather and Forecasting*, **4**, 323-334.

Kuo, Y-.H., and Reed, R.J., 1988: Numerical simulation of an explosively deepening cyclone in the Eastern Pacific. *Mon. Wea. Rev.*, **116**, 2081-2105.

Kuo, Y-.H., and S. Low-Nam, 1990: Prediction of nine explosive cyclones over the western Atlantic Ocean with a regional model. *Mon. Wea. Rev.*, **118**, 3-25.

Kuo, Y-.H., Reed, R.J., and S. Low-Nam, 1991: Effects of surface energy fluxes during the early development and rapid intensification stages of seven explosive cyclones in the Western Atlantic. *Mon. Wea. Rev.*, **119**, 457-476.

Nuss, W.A., and Anthes, R.A., 198?: A numerical investigation of low-level processes in rapid cyclogenesis. *Mon. Wea. Rev.*, **115**, 2728-2743.

Olanski, I., and Katzfey, J.J., 1987: Sensitivity of model simulations for a coastal cyclone. *Mon. Wea. Rev.*, **115**, 2792-2821.

Pauley, P.M., and Smith, P.J., 1988: Direct and indirect effects of latent heat release on a synoptic-scale wave system. *Mon. Wea. Rev.*, **116**, 1209-1235.

_____, Hoke, J.M., and Pecnick, M.J., 1991: Dynamic vs. diabatic forcing of rapid cyclogenesis: two case studies from NGM forecasts. Preprints of the first International Winter Storm Symposium, New Orleans, Amer. Meteor. Soc., 345-350.

Petterssen, S., 1956: *Weather Analysis and Forecasting, Vol I.*, 2nd ed., McGraw-Hill, 428 pp.

Robertson, F.R., and Smith, P. J., 1983: The impact of model moist processes on the energetics of extratropical cyclones. *Mon. Wea. Rev.*, **111**, 723-744.

Roebber, P.J., 1984: Statistical analysis and updated climatology of explosive cyclones. *Mon. Wea. Rev.*, **112**, 1577-1589.

Sanders, F., and Gyakum, J.R., 1980: Synoptic-dynamic climatology of the "bomb". *Mon. Wea. Rev.*, **108**, 1589-1606.

Sanders, F., 1986: Explosive cyclogenesis over the west-central North Atlantic Ocean, 1981-1984. part II: evaluation of LFM model performance. *Mon. Wea. Rev.*, **114**, 2207-2218.

_____, 1987: Skill of NMC operational dynamical models in prediction of explosive cyclogenesis. *Weather and Forecasting*, **2**, 322-336.

_____, and Auciello, E.P., 1989: Skill in prediction of explosive cyclogenesis over the western North Atlantic Ocean, 1987/88: a forecast checklist and NMC dynamical models. *Weather and Forecasting*, **4**, 157-172.

_____, 1990: Surface analysis over the oceans--searching for sea truth. *Weather and Forecasting*, **5**, 596-612.

Shapiro, R., 1975: Linear filtering. *Math. Comput.*, **29**, 1094-1097.

Tsou, C. H., Smith, P.J., and Pauley, P.M., 1987: A comparison of adiabatic and diabatic forcing in an intense extratropical cyclone system. *Mon. Wea. Rev.*,**115**, 763-786.

Uccellini, L. W., 1990: Processes contributing to the rapid development of extratropical cyclones, in *Extratropical Cyclones: The Erik Palmen Memorial Volume*, eds. Chester Newton and Eero O. Holopainen, Amer. Metero. Soc. Boston. 81-105.

VII. INITIAL DISTRIBUTION LIST

	No. Copies
1. Defense Technical Information Center Cameron Station Alexandria, VA 22304-6145	2
2. Library, Code 52 Naval Postgraduate School Monterey, CA 93943-5002	2
3. Chairman (Code MR/Hy) Department of Meteorology Naval Postgraduate School Monterey CA, 93943-5002	1
4. Professor Patricia M. Pauley (Code MR/Pa) Department of Meteorology Naval Postgraduate School Monterey, CA 93943-5002	2
5. Professor Carlyle H. Wash (Code MR/Wx) Department of Meteorology Naval Postgraduate School Monterey, CA 93943-5002	1
6. LT Frank W. Baker Fleet Numerical Oceanography Center Monterey, CA 93943-5005	
7. Commander Naval Oceanographic Command Stennis Space Center MS 39529-5000	1

8. Commanding Officer — 1
Fleet Numerical Oceanography Center
Monterey, CA 93943-5005

9. Commanding Officer — 1
Naval Oceanographic and Atmospheric Research Laboratory
Stennis Space Center
MS 39529-5004

10. Director — 1
Naval Oceanographic and Atmospheric Research Laboratory
Monterey, CA 93943-5006

11. Chief Of Naval Research — 1
800 North Quincy Street
Arlington, VA 22217

12. Office of Naval Research — 1
Naval Ocean Research and Development Activity
800 North Quincy Street
Arlington, VA 22217